Islet macrophages are the primary islet source of IGF-1 and improve glucose homeostasis following pancreatic beta-cell death

D. Nackiewicz[1], M. Dan[1], M. Speck[1], S. Z. Chow[1], J. A. Pospisilik[2], C. B. Verchere[1,3,4] and J. A. Ehses[1,4,5]

[1]Department of Surgery, Faculty of Medicine, University of British Columbia, BC Children's Hospital Research Institute, British Columbia, 950 W 28 Ave, Vancouver, V5Z 4H4, Canada

[2]Van Andel Research Institute, 333 Bostwick Ave. NE, Grand Rapids, MI 49503, USA

[3]Department of Pathology and Laboratory Medicine, BC Children's Hospital Research Institute, University of British Columbia, Vancouver, Canada

[4]Corresponding Contact

[5]Lead Contact

Lead Corresponding Contact:

Dr. Jan A. Ehses
Phone: +41 76 682 1336
Email: janehses@gmail.com
Twitter: @JanEhses

Corresponding Contact:

Dr. C. Bruce Verchere
Phone: +1 604-875-2490
E-mail: bverchere@bcchr.ca

SUMMARY

Pancreatic beta-cell death occurs in diabetes and contributes to hyperglycemia. By sampling the local tissue environment, macrophages act as critical gatekeepers of tissue homeostasis in health and disease. Here, we show that, following beta-cell death, islet macrophages acquire a state of heightened IGF-1 secretion, decreased proinflammatory cytokine expression, and transcriptome changes indicative of altered cellular metabolism. This was consistently observed across three rodent models of type 2 diabetes and islet macrophages were identified as the exclusive local source of IGF-1. Neither high blood glucose nor high fat diet altered the

activation state of these immune cells. Depletion of macrophages and IGF-1 neutralization both worsened streptozotocin-induced glucose tolerance, while adoptive transfer of bone-marrow-derived macrophages reduced glycemia and enhanced plasma insulin levels. Our data suggest increasing the number or functionality of islet macrophages may be an approach to preserve functional beta-cell mass in individuals with diabetes.

KEYWORDS

Pancreatic beta-cell, cell death, diabetes, efferocytosis, glucose homeostasis, high fat diet (HFD), IGF-1, inflammation, islet macrophage, islets, streptozotocin (STZ), tissue repair

INTRODUCTION

Pancreatic beta-cell death is a feature of both type 1 and 2 diabetes, contributing to inadequate insulin secretion and clinical hyperglycemia in both diseases. In type 1 diabetes, apoptotic and necrotic beta-cell death occur. While the immunological consequences of apoptotic cell death are unexplored, necrotic cell death is thought to initiate or further enhance the activation of antigen-presenting cells in response to released beta-cell factors, causing T cell priming and activation, and promoting autoimmunity (Wilcox et al., 2016). In contrast, in type 2 diabetes apoptotic beta-cell death is mainly associated with disease pathology (Halban et al., 2014).

Macrophages are versatile, plastic, innate immune cells essential to numerous biological processes. They participate in host defense, recognition of pathogens, initiation and resolution of inflammation, and maintenance of tissue homeostasis (Okabe and Medzhitov, 2016). In recent years, pancreatic stromal and islet macrophages have become increasingly well characterized. Islet macrophages in a resting state have an M1-like phenotype; they express

Il1b and *Tnf* transcripts, MHC-II, present antigens to T cells, are negative for CD206/CD301, and are derived from definitive hematopoiesis (Calderon et al., 2015, Ferris et al., 2017). In the presence of aggregates of islet amyloid polypeptide (IAPP), the pro-inflammatory state of these macrophages is enhanced, leading to IL-1 secretion that causes beta-cell dysfunction (Westwell-Roper et al., 2014). During extreme beta-cell injury or pancreatic damage in the absence of IAPP, however, islet macrophages can produce factors that support beta-cell replication and regeneration (Criscimanna et al., 2014, Riley et al., 2015, Xiao et al., 2014, Brissova et al., 2014).

The role of monocytes and macrophages in stromal cell regeneration has been studied in various tissues. For example, macrophage-derived insulin-like growth factor 1 (IGF-1) is required for skeletal muscle regeneration following injury (Lu et al., 2011, Tonkin et al., 2015). Various macrophage-derived growth factors are implicated in beta-cell regeneration in models of extreme beta-cell injury or during development, including TGFβ, CTGF, and IGF-2 (Riley et al., 2015, Xiao et al., 2014, Mussar et al., 2017). Here we focused on the role of macrophages in rodent models of type 2 diabetes and in response to moderate beta-cell death more representative of human disease pathology.

Because apoptotic cells promote a tissue repair program in macrophages (Bosurgi et al., 2017), and apoptosis is thought to be the main mechanism of beta-cell death in type 2 diabetes (Butler et al., 2003), we hypothesized that in the absence of IAPP aggregates, islet macrophages would skew to a tissue repair phenotype due to beta-cell death. Here, we thoroughly characterized resident islet macrophages and recruited monocyte cell populations and gene signatures in *db/db,* streptozotocin-treated (STZ), and high fat diet (HFD)-STZ-treated mice. IGF-1 expression was consistently increased in islet macrophages in all three models whereas pro-inflammatory cytokine gene expression was not increased. Transcriptome changes indicated an altered state of cellular metabolism mimicking efferocytosis. Furthermore,

macrophages positively regulated glucose homeostasis following beta-cell death *in vivo*, and IGF-1 neutralization exacerbated STZ-induced hyperglycemia through reduced insulin secretion. These findings suggest that increasing the number or functionality of regenerative macrophages may be used as an approach to preserve functional beta-cell mass in individuals with diabetes.

RESULTS

Islet macrophages in diabetic *db/db* mice express increased *Igf1* and decreased proinflammatory cytokines.

At 6 weeks of age, *db/db* mice had elevated body weight, were hyperglycemic, hyperglucagonemic, and hyperinsulinemic compared to BKS controls (Figures 1A-D). Between 8-11 weeks of age insulin levels declined (Figure 1D), indicative of beta-cell dysfunction and death (Puff et al., 2011, Medarova et al., 2005). Islet macrophages ($CD45^+Ly6C^-CD11B^+CD11C^+F4/80^+$) and recruited monocytes ($CD45^+Ly6C^+CD11B^+$) were evaluated in 8 and 11-week-old mice by flow cytometry (Figures 1E-H, S1C-F). Additionally, populations of other cells that were $CD45^+Ly6C^-$ (and $CD11B^-CD11C^-$/ $CD11B^+CD11C^-$/ $CD11B^-CD11C^+$: Figures 1I, S1G), $CD45^+Ly6C^+CD11B^-$ cell (Figures 1J, S1H), $CD45^-Ly6C^+$ cell (most likely endothelial cells; Figures 1K, S1I), and $CD45^-Ly6C^-$ cells (mainly endocrine cells; Figures 1L, S1J) were assessed. A trend towards increased numbers of $CD45^+$ cells in *db/db* islets at 8 weeks of age was mainly due to significantly increased numbers of islet macrophages (Figures 1F-G). No significant differences were observed in recruited monocytes or other immune cell populations, while $CD45^-Ly6C^+$ cell numbers were significantly reduced, and $CD45^-Ly6C^-$ cell numbers were increased (Figures 1H-L). Assessment of cytokine (*Il1a, Il1b, Il6, Tnf, Il1rn*) and growth-factor (*Igf1, Pdgfa, Tgfbi*) mRNA expression in islet macrophages indicated a decreased

proinflammatory state with 6-fold increased *Igf1* mRNA expression (Figure 1M). No differences in mRNA expression of these genes were detected in recruited monocytes (Figure S1A). $CD45^-$ $Ly6C^-$ cells also showed no differences in mRNA expression of cytokine genes, *Igf1, or Tgfbi*. However, *Pdgfa* mRNA was significantly reduced in *db/db* $CD45^-Ly6C^-$ cells (Figure S1B).

At 11 weeks of age, absolute numbers of $CD45^+$ cells in islets tended to be increased in *db/db* mice (Figures S1C-D). Interestingly, this difference was no longer due to differences in islet macrophage numbers (Figure S1E), and was mainly due to an increase in other $CD45^+Ly6C^-$ cells ($CD11B^-CD11C^-$/ $CD11B^+CD11C^-$/ $CD11B^-CD11C^+$, for example T cells, NK cells, B cells) and $CD45^+Ly6C^+CD11B^-$ cells (for example granulocytes, plasma cells, NK cells, or T-cell subsets, Figures S1G-H). Islet-macrophage cytokine and growth-factor mRNA expression showed a similar trend to data from 8-week-old *db/db* mice (Figure S1K).

Thus, islet macrophage numbers are increased in 8-week-old *db/db* mice, and gene expression indicates a state of increased *Igf1* expression, and interestingly, a decreased proinflammatory state.

Islet macrophages in HFD+STZ mice express increased *Igf1, Pdgfa, and Tgfbi.*

Islet macrophages and recruited monocytes were evaluated in another rodent model of type 2 diabetes, the HFD+STZ mouse. Mice were fed a HFD for either 6 or 12 weeks, followed by STZ-induced beta-cell death (Figure 2A). At the end of treatment, 6-week HFD, 12-week HFD, and 12-week HFD+STZ mice had increased body weight compared to chow fed mice (Figure 2B). Non-fasting blood glucose was increased in 6-week and 12-week HFD+STZ mice (Figure 2C), and glucose tolerance was impaired (Figures 2D-E). Numbers of $CD45^+$ cells in islets were significantly increased in 6-week and 12-week HFD+STZ mice, due to increased numbers of islet macrophages, recruited monocytes and other $CD45^+Ly6C^+$ cells (Figures 2F-I,

S2A-B). Comparable to islet macrophage mRNA expression in *db/db* mice, 6 and 12-week HFD+STZ mice had increased *Igf1, Pdgfa*, and *Tgfbi* mRNA expression in islet macrophages, but no change in expression of proinflammatory cytokines (Figure 2J). Interestingly, increased time on HFD tended to enhance the expression of *Pdgfa*, and *Tgfbi*, while further suppressing pro-inflammatory cytokine expression (Figure 2J). No differences in mRNA expression of these genes were detected in recruited monocytes (Figure 2K).

Similar to 11-week-old *db/db* mice, increased numbers of other $CD45^{+}Ly6C^{+}$ cells were also detected in 6-week and 12-week HFD+STZ mice compared to controls (Figure S2B). No differences in islet $CD45^{-}Ly6C^{+}$ cell numbers were found (Figure S2C), while cell numbers of $CD45^{-}Ly6C^{-}$ were higher in 12-week HFD+STZ compared to control islets (Figure S2D). Like those of *db/db* mice, $CD45^{-}Ly6C^{+}$ cells and $CD45^{-}Ly6C^{-}$ cells of HFD+STZ mice showed no differences in mRNA expression of cytokines or growth factor genes (Figures S2E-F).

In summary, HFD+STZ mice show similarities to 8-week-old *db/db* mice, in that their islet macrophage numbers are increased and their gene expression pattern indicates a non-proinflammatory state of activation and increased growth factor expression.

Islet macrophages in mice challenged with multiple low-dose STZ exhibit a gene set shift indicative of enhanced metabolism and secrete IGF-1.

To determine the mechanism causing islet macrophage skewing in *db/db* and HFD+STZ mice, we studied islet macrophages and recruited monocytes following STZ-induced beta-cell death *in vivo* and *ex vivo*. Body weight and non-fasting blood glucose were unchanged up to 3 weeks post STZ (Figures 3A-B). Similar to *db/db* and HFD+STZ mice, islet $CD45^{+}$ cells, islet macrophages, and recruited monocytes were increased following STZ, with significant changes detectable at 1 and 2 weeks (Figures 3C-F). Islet macrophages showed decreased *Il1b* and *Tnf*

mRNA expression and increased *Il1rn, Igf1,* and *Tgfbi* mRNA expression (Figure 3G). No differences in mRNA expression of these genes were detected in recruited monocytes (Figure 2H).

To obtain a broader unbiased view of the changes in islet macrophages following STZ, we performed a transcriptome analysis of isolated islet macrophages at 2 weeks post STZ. The obtained gene expression profile was consistent with phagocytic immune cells (Figure 3I). Cd74 (encoding part of MHC class II) was the most abundant transcript detected. Lyz2 (also known as LysM) and Ctsd (cathepsin D gene), both associated with lysozyme, were also highly expressed. Gene Set Enrichment Analysis (GSEA) using the curated canonical pathways databases highlighted gene enrichment in various pathways involved in cellular metabolism and the metabolism of small molecules and proteins (Table S1). Interestingly, a heat map of the top 25 enriched genes resulted in IGF-1 having the highest score (3.47) among all enriched genes (Figure 3J). An enrichment map of the main altered pathways highlighted genes involved in increased ATP production (oxidative phosphorylation), increased sugar metabolism, and increased lipid metabolism, in parallel with increased lysosome and protein degradation activity (Figure 3K). Taken together, the transcriptome of islet macrophages from STZ-treated mice indicates enhanced metabolism of sugar and lipid substrates and polarization towards a tissue repair phenotype.

To confirm that STZ was causing beta-cell apoptosis, the numbers of $TUNEL^{+}Insulin^{+}$ cells were assessed at 1 and 2 weeks post STZ, with a 3-fold increase found at 2 weeks (Figures 3L-M). Finally, isolated islet macrophages secreted IGF-1 protein as assessed by ELISPOT, while $CD45^{-}Ly6C^{+}$ (most likely endothelial cells) and $CD45^{-}Ly6C^{-}$ cells (mainly endocrine cells) did not (Figures 3N-O).

Islet macrophage depletion decreases *Igf1* expression and beta-cell proliferation following STZ-induced beta-cell death *ex vivo*.

To isolate primary beta-cell STZ effects from secondary effects (e.g. elevated postprandial glucose) that may modulate islet macrophage gene expression *in vivo*, experiments were performed on isolated islets. Treatment of islets with increasing concentrations of STZ (0.25 - 4 mM) paralleled our *in vivo* results, causing a decrease in *Il1b* mRNA expression, and significantly increased *Tgfbi* and *Pdgfa* mRNA expression (Figure 4A). Whole islet *Il1rn* and *Igf1* mRNA expression also tended to increase. Beta-cell *Ins1* and *Ins2* expression were unchanged, while *Pdx1* expression was increased by 4 mM STZ treatment. To determine the contribution of islet macrophages to these gene expression changes, islet macrophages were depleted using islets isolated from CD11c-DTR mice treated with diphtheria toxin (DT). Macrophage depletion following DT was confirmed by flow cytometry (Figure 4B). Depletion of islet macrophages completely abolished the STZ-induced increase in *Igf1* mRNA expression (Figure 4C), while having no effect on beta-cell mRNA levels (*Ins1, Ins2, Pdx1*). Our data further indicate that macrophages are the main source of *Tgfbi* transcript levels in islets (Figure 4C). As previously shown (Westwell-Roper et al., 2014, Ferris et al., 2017, Nackiewicz et al., 2014), islet macrophages are also the main contributors to islet *Il1b* and *Tnf* expression.

STZ treated islets also had increased numbers of $TUNEL^{+}Insulin^{+}$ cells (Figures 4D-E), with no effect on $EdU^{+}Insulin^{+}$ cells (Figures 4F-G). Depletion of islet macrophages reduced $EdU^{+}Insulin^{+}$ cells (Figure 4G). STZ did not increase *Igf1* mRNA expression or protein secretion, or affect proliferation or apoptosis in bone marrow derived macrophages (BMDMs; Figures S3A-D). These data support the conclusion that primary beta-cell STZ effects stimulate macrophage *Igf1* mRNA expression.

Macrophages and IGF-1 positively regulate glucose homeostasis in mice following STZ.

To investigate the role of macrophages during beta-cell death *in vivo,* we depleted phagocytic cells with clodronate loaded liposomes during, and immediately following, STZ (Figure 5A). There were no differences in body weight (Figure 5B) between treatment groups, while non-fasting blood glucose was significantly elevated at the end of the treatment in the STZ group that received clodronate loaded liposomes versus the control group (Figure 5C). Liposome (PBS and clodronate loaded) STZ treated mice also showed impaired glucose tolerance (Figures 5D-E), despite no difference in serum insulin levels during the IPGTT (Figure 5F). This is consistent with a previously described effect of liposomes themselves on macrophage function (Pervin et al., 2016, Ma et al., 2011), or might have been due to macrophage depletion with PBS-liposomes (Weisser et al., 2011).

Next, we investigated if adoptively transferred macrophages could protect mice from STZ-induced hyperglycemia. We used BMDMs that were starved of L929-conditioned media, a source of macrophage colony-stimulating factor (M-CSF), nerve growth factor (NGF) and other undefined factors (Moore et al., 1980, Pantazis et al., 1977, Warren and Ralph, 1986), for either 24 hours or 72 hours (Figure 5G). Both macrophage preparations produced non-fasting blood glucose levels lower than those of mice that were treated only with STZ (Figure 5I), with no effect on their body weights (Figure 5H). Concordantly, STZ-treated mice that received macrophages demonstrated better glucose tolerance following an oral glucose tolerance test (Figures 5J-K). In another cohort of mice, we evaluated non-fasting serum insulin on day 12 following the last injection of macrophages (Figure 5L) and pancreatic insulin content on the day of sacrifice (Figure 5M). As in the previous cohort, there was no change in body weight (Figure S4A) and post-STZ non-fasting blood glucose was lower in macrophage-treated mice (Figure S4B). Serum insulin was significantly higher in the STZ group that received macrophages, while pancreatic insulin content was 3-fold lower in both groups that were treated with STZ. We also

checked whole pancreas mRNA expression and saw a significant downregulation of *Ins1* and *Ins2,* with no change in *Pdx1,* in both sets of STZ-treated animals compared to controls (Figure S4C). These data support the conclusion that macrophages positively regulate beta-cell function *in vivo* following STZ-induced beta-cell death.

Finally, we investigated whether IGF-1 neutralization impacts glucose homeostasis during STZ-induced beta-cell death (Figure 5N). Non-fasting blood glucose following IGF-1 neutralization was lower compared to the control IgG group (Figure 5P), with no effect on body weights (Figure 5O). Conversely, STZ treated mice injected with the IGF-1-neutralizing antibody had exacerbated glucose intolerance and lower insulin levels (Figures 5R-T). Thus, post STZ-induced beta-cell death, IGF-1 signaling acts in a compensatory manner to maintain beta-cell insulin secretion *in vivo.*

Discussion

Islet macrophage activation and function are context-dependent (Morris, 2017, Eguchi and Nagai, 2017). While islet macrophages are pro-inflammatory and major contributors to islet IL-1β in the presence of IAPP aggregates (Masters et al., 2010, Westwell-Roper et al., 2016) or when exposed to toll-like receptor ligands (Nackiewicz et al., 2014), macrophages can also support pancreas remodeling and beta-cell proliferation under certain conditions (Morris, 2017). Our data indicate a beneficial role of islet macrophages in the context of mouse models of type 2 diabetes and beta-cell death. In three different mouse models of beta-cell death, expression of pro-inflammatory cytokines was consistently decreased, and that of *Igf1* was consistently increased in islet macrophages. Macrophage depletion and adoptive transfer experiments supported their role in maintaining glucose homeostasis following beta-cell death. Finally, islet macrophages were the sole contributors to islet IGF-1 expression and secretion, and IGF-1

acted in a compensatory manner to maintain beta-cell insulin secretion in the face of beta-cell death.

Recent research on islet macrophages has focused mainly on their characterization in the resting state (Weitz et al., 2018), their role in type 1 diabetes (Carrero et al., 2017), and their role in beta-cell proliferation (Xiao and Gittes, 2015, Morris, 2017). Studies by Unanue and colleagues demonstrated that islet macrophages in mice in a resting state are mainly pro-inflammatory and are derived from definitive hematopoiesis (Ferris et al., 2017, Calderon et al., 2015). Other studies have investigated macrophage-dependent beta-cell proliferation during pancreas development (Mussar et al., 2017), in models of beta-cell ablation (Criscimanna et al., 2014, Riley et al., 2015), after pancreatic duct ligation (Xiao et al., 2014), or in islets transiently overexpressing vascular endothelial growth factor-A (VEGF-A) (Brissova et al., 2014). Multiple mechanisms of macrophage-dependent beta-cell proliferation were proposed, implicating roles for growth factors such as TGFβ, CTGF, and IGF-2. Importantly, our study is the first to show that islet macrophages can change their polarization state to one that resembles that of macrophages involved in wound healing and tissue repair (Wynn and Vannella, 2016, Lech and Anders, 2013), even in the presence of severe hyperglycemia (*db/db)* or during HFD feeding (STZ+HFD). Furthermore, these macrophages help limit the worsening of glucose tolerance in an acute model of beta-cell death.

Transcriptome analysis of islet macrophages following beta-cell death was consistent with biological pathways regulated in macrophages undergoing efferocytosis (Voll et al., 1997, Henson, 2017). This included increased expression of genes involved in energy substrate utilization and ATP production (oxidative phosphorylation), in parallel with increased lysosome and protein degradation activity. Efferocytosis is known to induce an anti-inflammatory, reparative state in macrophages and has been increasingly studied in cardiovascular diseases such as atherosclerosis (Brophy et al., 2017). These data help explain the changes seen in islet macrophages when beta-cell death was combined with HFD feeding. The enhanced skewing

towards a non-inflammatory, tissue repair phenotype could be the result of an increased availability of an energy source (fats, glucose, sucrose), supporting the energy needs of macrophages undergoing efferocytosis. Indeed, changes in cellular metabolism leading to functional programming of phagocytic macrophages is a subject of considerable current interest: our data highlight potential pathways that could be targeted to promote islet macrophages with tissue-regenerative properties.

Mice with beta-cell deficiency of the IGF-1 receptor were previously shown to have dysregulated glucose-stimulated insulin secretion, with no effects on beta-cell mass, leading to impaired glucose tolerance (Kulkarni et al., 2002, Xuan et al., 2002), Our data are in agreement with these studies, suggesting that islet macrophage IGF-1 contributes to beta-cell function and glucose homeostasis. Further, our findings indicate that islet macrophages are by far the major, if not sole, source of IGF-1 produced within the islet.

A report by Eguchi and colleagues suggested that islet macrophages in diabetic *db/db* mice are in a proinflammatory state (Eguchi et al., 2012), with increased pro-inflammatory gene expression and increased numbers of CD11B+Ly6C+ cells infiltrating islets. By contrast, our fuller characterization of the islet macrophage gene expression profile in BKS versus *db/db* mice has revealed decreased proinflammatory gene expression and increased expression of regenerative genes such as IGF-1. Increased whole-islet cytokine mRNA expression in that study could simply be due to increased numbers of islet macrophages, because islet macrophages express *Il1b* and *Tnf* at ~10^4-fold higher levels than endocrine cells (Figures 1, S1-2 and Nackiewicz et al., 2014). While depletion of islet macrophages in that study did improve insulin secretion, it is entirely possible that an alternatively activated macrophage could be causing beta-cell dedifferentiation in an attempt to regenerate damaged tissue. We also cannot exclude the possibility that differences in the gut microbiota may have contributed to this discrepancy, since the *db/db* mice in these two studies were derived from different sources. In support of our findings, a more recent study found that a potent inhibitor of NLRP3-induced IL-

1β secretion had no effect on *db/db* disease pathogenesis (Kammoun et al., 2018). In any case, our data provide new insight into the functional state of islet macrophages in diabetes and during beta-cell death.

Our data also have therapeutic implications relevant to type 1 or 2 diabetes. Because islet macrophages can still change their phenotype even in the presence of severe hyperglycemia or during HFD feeding, increasing their number or functionality might be an approach to preserving functional beta-cell mass in individuals with diabetes. Furthermore, mechanistic insight into how IGF-1 acts in a paracrine or autocrine manner in islets could lead to new ways to mimic its actions to treat diabetes. For example, Han et al., 2016 recently demonstrated that IGF-1 secreted from macrophages following phagocytosis of apoptotic cells could enhance uptake of microvesicles by non-professional phagocytes and dampen their inflammatory response. Autocrine effects of IGF-1 are known to influence phagocytic activity and propagate an M2-like activated macrophage phenotype (Spadaro et al., 2017, Higashi et al., 2016). Future study should focus on understanding the paracrine/autocrine mechanism of action of macrophage-derived IGF-1 in the islet, and the translation of these findings towards preservation of functional beta-cell mass in individuals with diabetes.

Limitations of the study

Currently available techniques do not allow us to selectively manipulate islet macrophages *in vivo*. To minimize the impact of this limitation, we employed a number of *in vivo* and *in vitro* techniques and made use of a model that limits cell death to beta cells of the pancreatic islet. Macrophages were depleted both *in vivo* and *ex vivo* and this was complemented by adoptive cell transfer experiments. The data herein support the conclusion that macrophages positively regulate beta-cell insulin secretion *in vivo* following STZ-induced beta-cell death. While the lack of effect on insulin content in our adoptive transfer experiment (Figure 5M) suggests an effect on insulin secretory capacity rather than beta-cell proliferation or

mass, this remains an open question. Further, the impact of IGF-1 neutralization was studied *in vivo* with effects on glucose tolerance that were consistent with macrophage depletion. This finding suggests that macrophage-derived IGF-1 is important in limiting beta-cell functional damage post-STZ. While it was beyond the scope of this study to determine the cell-specific actions of macrophage-derived IGF-1, effects on insulin secretion and glucose homeostasis may be due to direct effects of IGF-1 on beta cells (Kulkarni et al., 2002, Dheen et al., 1996), or indirect effects on alpha-cell glucagon secretion (Mancuso et al., 2017), or on other islet cell types to limit tissue inflammation (Han et al., 2016).

Acknowledgments

We are grateful to Dr. Laura Sly, Dr. Francis Lynn, Dr. Heather Denroche, and Dr. Paul Orban from the BC Children's Hospital Research Institute for helpful discussions and suggestions during the conduct of the study, to Mitsuhiro Komba from the Islet Core Facility, Dr. Lisa Xu from the Flow Core Facility, Dr. Jingsong Wang and Dr**.** Bao Ping Song from the Histology and Imaging Core Facilities, Dr. Derek Dai and Dr. Galina Soukhatcheva for their technical assistance, and to Ryan Vander Werff from the UBC Biomedical Research Centre Sequencing Core for help with RNA-seq sequencing. This work was supported by a grant from the Canadian Institutes of Health Research (CIHR). D.N. was supported by a CIHR-Vanier Canada Graduate Scholarship. C.B.V. is supported by an investigator award from BC Children's Hospital and the Irving K. Barber Chair in Diabetes Research.

Author Contributions

Conceptualization, D.N. and J.A.E.; Methodology, D.N., M.D. and J.A.E; Investigation, D.N., M.D., M.S., S.Z.C.; Formal analysis, D.N., J.A.P, J.A.E; Resources J.A.P., J.A.E., C.B.V.; Writing– Original Draft, D.N. and J.A.E.; Writing– Review & Editing, D.N., J.A.E., J.A.P., C.B.V.; Visualization, D.N.; Funding Acquisition, J.A.E. and C.B.V.; Supervision, J.A.E. and C.B.V.

Declaration of Interests

The authors declare no competing interests.

References

Bosurgi, L., Cao, Y.G., Cabeza-Cabrerizo, M., Tucci, A., Hughes, L.D., Kong, Y., Weinstein, J.S., Licona-Limon, P., Schmid, E.T., Pelorosso, F., et al. (2017). Macrophage function in tissue repair and remodeling requires IL-4 or IL-13 with apoptotic cells. Science *356*, 1072–1076.

Brissova, M., Aamodt, K., Brahmachary, P., Prasad, N., Hong, J.-Y., Dai, C., Mellati, M., Shostak, A., Poffenberger, G., Aramandla, R., et al. (2014). Islet microenvironment, modulated by vascular endothelial growth factor-A signaling, promotes β cell regeneration. Cell Metab. *19*, 498–511.

Brophy, M.L., Dong, Y., Wu, H., Rahman, H.N.A., Song, K., and Chen, H. (2017). Eating the Dead to Keep Atherosclerosis at Bay. Front. Cardiovasc. Med. *4*, 2.

Butler, A.E., Janson, J., Bonner-Weir, S., Ritzel, R., Rizza, R.A., and Butler, P.C. (2003). Beta-cell deficit and increased beta-cell apoptosis in humans with type 2 diabetes. Diabetes *52*, 102–110.

Calderon, B., Carrero, J.A., Ferris, S.T., Sojka, D.K., Moore, L., Epelman, S., Murphy, K.M., Yokoyama, W.M., Randolph, G.J., and Unanue, E.R. (2015). The pancreas anatomy conditions the origin and properties of resident macrophages. J. Exp. Med. *212*, 1497–1512.

Carrero, J.A., McCarthy, D.P., Ferris, S.T., Wan, X., Hu, H., Zinselmeyer, B.H., Vomund, A.N., and Unanue, E.R. (2017). Resident macrophages of pancreatic islets have a seminal role in the initiation of autoimmune diabetes of NOD mice. Proc. Natl. Acad. Sci. U. S. A. *114*, E10418–E10427.

Criscimanna, A., Coudriet, G.M., Gittes, G.K., Piganelli, J.D., and Esni, F. (2014). Activated Macrophages Create Lineage-Specific Microenvironments for Pancreatic Acinar- and β-Cell Regeneration in Mice. Gastroenterology *147*, 1106–1118.e11.

Dheen, S.T., Rajkumar, K., and Murphy, L.J. (1996). Effects of insulin-like growth factors (IGF) on pancreatic islet function in IGF binding protein-1 transgenic mice. Diabetologia *39*, 1249–1254.

Eguchi, K., and Nagai, R. (2017). Islet inflammation in type 2 diabetes and physiology. J. Clin. Invest. *127*, 14–23.

Eguchi, K., Manabe, I., Oishi-Tanaka, Y., Ohsugi, M., Kono, N., Ogata, F., Yagi, N., Ohto, U., Kimoto, M., Miyake, K., et al. (2012). Saturated fatty acid and TLR signaling link β cell dysfunction and islet inflammation. Cell Metab. *15*, 518–533.

Ferris, S.T., Zakharov, P.N., Wan, X., Calderon, B., Artyomov, M.N., Unanue, E.R., and Carrero, J.A. (2017). The islet-resident macrophage is in an inflammatory state and senses microbial products in blood. J. Exp. Med. *214*, jem.20170074.

Halban, P.A., Polonsky, K.S., Bowden, D.W., Hawkins, M.A., Ling, C., Mather, K.J., Powers, A.C., Rhodes, C.J., Sussel, L., and Weir, G.C. (2014). β-Cell Failure in Type 2 Diabetes: Postulated Mechanisms and Prospects for Prevention and Treatment. J. Clin. Endocrinol. Metab. *99*, 1983–1992.

Han, C.Z., Juncadella, I.J., Kinchen, J.M., Buckley, M.W., Klibanov, A.L., Dryden, K., Onengut-Gumuscu, S., Erdbrügger, U., Turner, S.D., Shim, Y.M., et al. (2016). Macrophages redirect phagocytosis by non-professional phagocytes and influence inflammation. Nature *539*, 570–574.

Henson, P.M. (2017). Cell Removal: Efferocytosis. Annu. Rev. Cell Dev. Biol. *33*, 127–144.

Higashi, Y., Sukhanov, S., Shai, S.-Y., Danchuk, S., Tang, R., Snarski, P., Li, Z., Lobelle-Rich, P., Wang, M., Wang, D., et al. (2016). Insulin-Like Growth Factor-1 Receptor Deficiency in Macrophages Accelerates Atherosclerosis and Induces an Unstable Plaque Phenotype in Apolipoprotein E-Deficient Mice. Circulation *133*, 2263–2278.

Kammoun, H.L., Allen, T.L., Henstridge, D.C., Barre, S., Coll, R.C., Lancaster, G.I., Cron, L., Reibe, S., Chan, J.Y., Bensellam, M., et al. (2018). Evidence against a role for NLRP3-driven islet inflammation in db/db mice. Mol. Metab. *10*, 66–73.

Kulkarni, R.N., Holzenberger, M., Shih, D.Q., Ozcan, U., Stoffel, M., Magnuson, M. a, and Kahn, C.R. (2002). beta-cell-specific deletion of the Igf1 receptor leads to hyperinsulinemia and glucose intolerance but does not alter beta-cell mass. Nat. Genet. *31*, 111–115.

Lech, M., and Anders, H.J. (2013). Macrophages and fibrosis: How resident and infiltrating mononuclear phagocytes orchestrate all phases of tissue injury and repair. Biochim. Biophys. Acta - Mol. Basis Dis. *1832*, 989–997.

Love, M.I., Huber, W., and Anders, S. (2014). Moderated estimation of fold change and dispersion for RNA-seq data with DESeq2. Genome Biol. *15*, 550.

Lu, H., Huang, D., Saederup, N., Charo, I.F., Ransohoff, R.M., and Zhou, L. (2011). Macrophages recruited via CCR2 produce insulin-like growth factor-1 to repair acute skeletal muscle injury. FASEB J. *25*, 358–369.

Ma, H.M., Wu, Z., and Nakanishi, H. (2011). Phosphatidylserine-containing liposomes suppress inflammatory bone loss by ameliorating the cytokine imbalance provoked by infiltrated macrophages. Lab. Investig. *91*, 921–931.

Mancuso, E., Mannino, G.C., Fatta, C. Di, Fuoco, A., Spiga, R., Andreozzi, F., and Sesti, G. (2017). Insulin-like growth factor-1 is a negative modulator of glucagon secretion. Oncotarget *8*, 51719–51732.

Masters, S.L., Dunne, A., Subramanian, S.L., Hull, R.L., Tannahill, G.M., Sharp, F.A., Becker,

C., Franchi, L., Yoshihara, E., Chen, Z., et al. (2010). Activation of the NLRP3 inflammasome by islet amyloid polypeptide provides a mechanism for enhanced IL-1β in type 2 diabetes. Nat. Immunol. *11*, 897–904.

Medarova, Z., Bonner-Weir, S., Lipes, M., and Moore, A. (2005). Imaging beta-cell death with a near-infrared probe. Diabetes *54*, 1780–1788.

Moore, R.N., Oppenheim, J.J., Farrar, J.J., Carter, C.S., Waheed, A., and Shadduck, R.K. (1980). Production of lymphocyte-activating factor (Interleukin 1) by macrophages activated with colony-stimulating factors. J. Immunol. *125*, 1302–1305.

Mootha, V.K., Lindgren, C.M., Eriksson, K.-F., Subramanian, A., Sihag, S., Lehar, J., Puigserver, P., Carlsson, E., Ridderstråle, M., Laurila, E., et al. (2003). PGC-1α-responsive genes involved in oxidative phosphorylation are coordinately downregulated in human diabetes. Nat. Genet. *34*, 267–273.

Morris, D.L. (2017). Minireview : Emerging Concepts in Islet Macrophage Biology in Type 2 Diabetes. Mol. Endocrinol. *29*, 946–962.

Mussar, K., Pardike, S., Hohl, T.M., Hardiman, G., Cirulli, V., and Crisa, L. (2017). A CCR2+ myeloid cell niche required for pancreatic β cell growth. JCI Insight *2*.

Nackiewicz, D., Dan, M., He, W., Kim, R., Salmi, A., Rütti, S., Westwell-Roper, C., Cunningham, A., Speck, M., Schuster-Klein, C., et al. (2014). TLR2/6 and TLR4-activated macrophages contribute to islet inflammation and impair beta cell insulin gene expression via IL-1 and IL-6. Diabetologia *57*, 1645–1654.

Okabe, Y., and Medzhitov, R. (2016). Tissue biology perspective on macrophages. Nat. Immunol. *17*, 9–17.

Pantazis, N.J., Blanchard, M.H., Arnason, B.G., and Young, M. (1977). Molecular properties of the nerve growth factor secreted by L cells. Proc. Natl. Acad. Sci. U. S. A. *74*, 1492–1496.

Pervin, M., Golbar, H.M., Bondoc, A., Izawa, T., Kuwamura, M., and Yamate, J. (2016). Transient effects of empty liposomes on hepatic macrophage populations in rats. J. Toxicol. Pathol. *29*, 139–144.

Puff, R., Dames, P., Weise, M., Göke, B., Seissler, J., Parhofer, K.G., and Lechner, A. (2011). Reduced Proliferation and a High Apoptotic Frequency of Pancreatic Beta Cells Contribute to Genetically-determined Diabetes Susceptibility of db/db BKS Mice. Horm. Metab. Res. *43*, 306–311.

Riley, K.G., Pasek, R.C., Maulis, M.F., Dunn, J.C., Bolus, W.R., Kendall, P.L., Hasty, A.H., and Gannon, M. (2015). Macrophages are essential for CTGF-mediated adult β-cell proliferation after injury. Mol. Metab. *4*, 584–591.

Spadaro, O., Camell, C.D., Bosurgi, L., Nguyen, K.Y., Youm, Y.-H., Rothlin, C. V., and Dixit, V.D. (2017). IGF1 Shapes Macrophage Activation in Response to Immunometabolic Challenge. Cell Rep. *19*, 225–234.

Subramanian, A., Tamayo, P., Mootha, V.K., Mukherjee, S., Ebert, B.L., Gillette, M.A., Paulovich, A., Pomeroy, S.L., Golub, T.R., Lander, E.S., et al. (2005). Gene set enrichment analysis: a knowledge-based approach for interpreting genome-wide expression profiles. Proc. Natl. Acad. Sci. U. S. A. *102*, 15545–15550.

Tonkin, J., Temmerman, L., Sampson, R.D., Gallego-Colon, E., Barberi, L., Bilbao, D.,

Schneider, M.D., Musarò, A., and Rosenthal, N. (2015). Monocyte/Macrophage-derived IGF-1 Orchestrates Murine Skeletal Muscle Regeneration and Modulates Autocrine Polarization. Mol. Ther. *23*, 1189–1200.

Voll, R.E., Herrmann, M., Roth, E.A., Stach, C., Kalden, J.R., and Girkontaite, I. (1997). Immunosuppressive effects of apoptotic cells. Nature *390*, 350–351.

Warren, M.K., and Ralph, P. (1986). Macrophage growth factor CSF-1 stimulates human monocyte production of interferon, tumor necrosis factor, and colony stimulating activity. J. Immunol. *137*, 2281–2285.

Weisser, S.B., Brugger, H.K., Voglmaier, N.S., McLarren, K.W., van Rooijen, N., and Sly, L.M. (2011). SHIP-deficient, alternatively activated macrophages protect mice during DSS-induced colitis. J Leukoc Biol *90*, 483–492.

Weitz, J.R., Makhmutova, M., Almaça, J., Stertmann, J., Aamodt, K., Brissova, M., Speier, S., Rodriguez-Diaz, R., and Caicedo, A. (2018). Mouse pancreatic islet macrophages use locally released ATP to monitor beta cell activity. Diabetologia *61*, 182–192.

Westwell-Roper, C., Denroche, H.C., Ehses, J.A., and Verchere, C.B. (2016). Differential Activation of Innate Immune Pathways by Distinct Islet Amyloid Polypeptide (IAPP) Aggregates. J. Biol. Chem. *291*, 8908–8917.

Westwell-Roper, C.Y., Ehses, J.A., and Verchere, C.B. (2014). Resident Macrophages Mediate Islet Amyloid Polypeptide–Induced Islet IL-1β Production and β-Cell Dysfunction. Diabetes *63*, 1698–1711.

Wilcox, N.S., Rui, J., Hebrok, M., and Herold, K.C. (2016). Life and death of β cells in Type 1 diabetes: A comprehensive review. J. Autoimmun. *71*, 51–58.

Wynn, T.A., and Vannella, K.M. (2016). Macrophages in Tissue Repair, Regeneration, and Fibrosis. Immunity *44*, 450–462.

Xiao, X., and Gittes, G.K. (2015). Concise Review: New Insights Into the Role of Macrophages in β-Cell Proliferation. Stem Cells Transl. Med. *4*, 655–658.

Xiao, X., Gaffar, I., Guo, P., Wiersch, J., Fischbach, S., Peirish, L., Song, Z., El-Gohary, Y., Prasadan, K., Shiota, C., et al. (2014). M2 macrophages promote beta-cell proliferation by up-regulation of SMAD7. Proc. Natl. Acad. Sci. U. S. A. *111*, E1211-20.

Xuan, S., Kitamura, T., Nakae, J., Politi, K., Kido, Y., Fisher, P.E., Morroni, M., Cinti, S., White, M.F., Herrera, P.L., et al. (2002). Defective insulin secretion in pancreatic beta cells lacking type 1 IGF receptor. J. Clin. Invest. *110*, 1011–1019.

Younesy, H., Möller, T., Lorincz, M.C., Karimi, M.M., and Jones, S.J. (2015). VisRseq: R-based visual framework for analysis of sequencing data. BMC Bioinformatics *16*, S2.

Figure 1

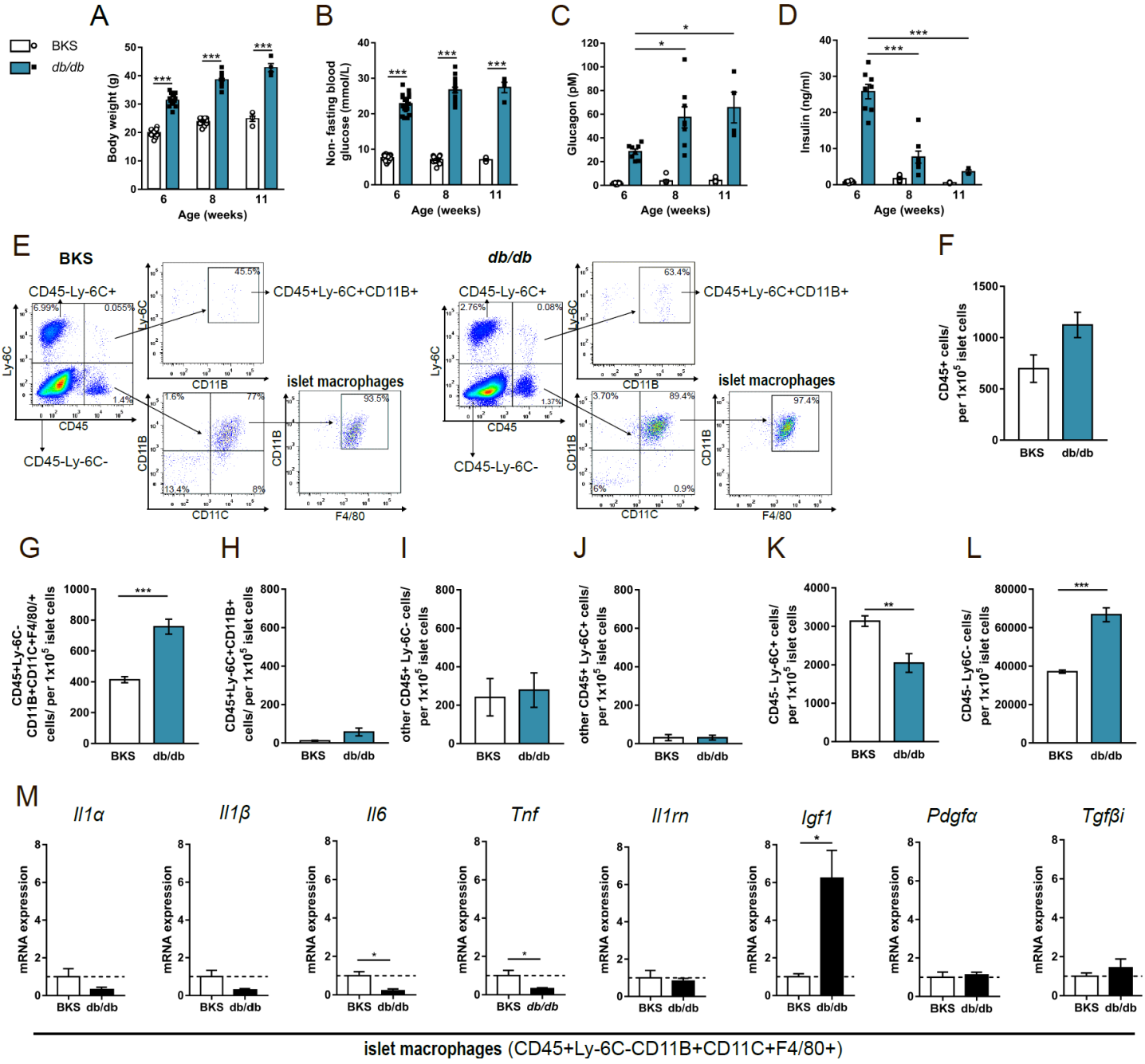

Figure 1

Islet macrophages in diabetic *db/db* mice express *Igf1* and decreased proinflammatory cytokines.

(A) Body weight of 6-11-week-old male BKS and *db/db* mice.

(B) Non-fasting blood glucose levels of 6-11-week-old BKS and *db/db* mice.

(A-B) n=17-18 mice for 6-8-week-old groups, n=4 mice for 11-week-old group; ***p < 0.001 versus BKS, Student's t test.

(C) Non-fasting glucagon levels; n=8 mice for 6-8-week-old groups, n=4 mice for 11-week-old group; *p < 0.05 versus 6 wks old *db/db*, one-way ANOVA with Dunnett's multiple comparisons test.

(D) Non-fasting insulin levels; n=8 mice for 6-8-week-old group, n=3-4 mice for 11-week-old group; ***p < 0.001 versus 6 wks old *db/db*, one-way ANOVA with Dunnett's multiple comparisons test.

(E) Representative flow cytometry profiles and gating strategy for cell sorting of dispersed islets from 8-week-old BKS and *db/db* mice.

Fractions of (F) CD45+ cells, (G) CD45+Ly-6C-CD11B+CD11C+F4/80+ cells, (H) CD45+Ly-6C+CD11B+ cells, (I) other CD45+Ly-6C- cells, (J) other CD45+Ly-6C+ cells, (K) CD45-Ly-6C+ cells, (L) and CD45-Ly-6C- cells in islets of 8-week-old BKS and *db/db* mice; (F-L) n=4, 2-4 mice pooled to obtain 556 +/- 52 islets per sample (n); **p < 0.01, ***p < 0.001 versus BKS, Student's t test.

(M) qPCR of islet macrophages (G). Relative expression levels of *Il1α*, *Il1β*, *Tnf*, *Il6*, *Il1rn*, *Igf1*, *Pdgfα*, and *Tgfβi* expressed as fold control (BKS); n=4, 2-4 mice pooled per sample (n); *p < 0.05, Student's t test.

Bar graphs or data points represent mean ± SEM.

See also Figure S1.

Figure 2

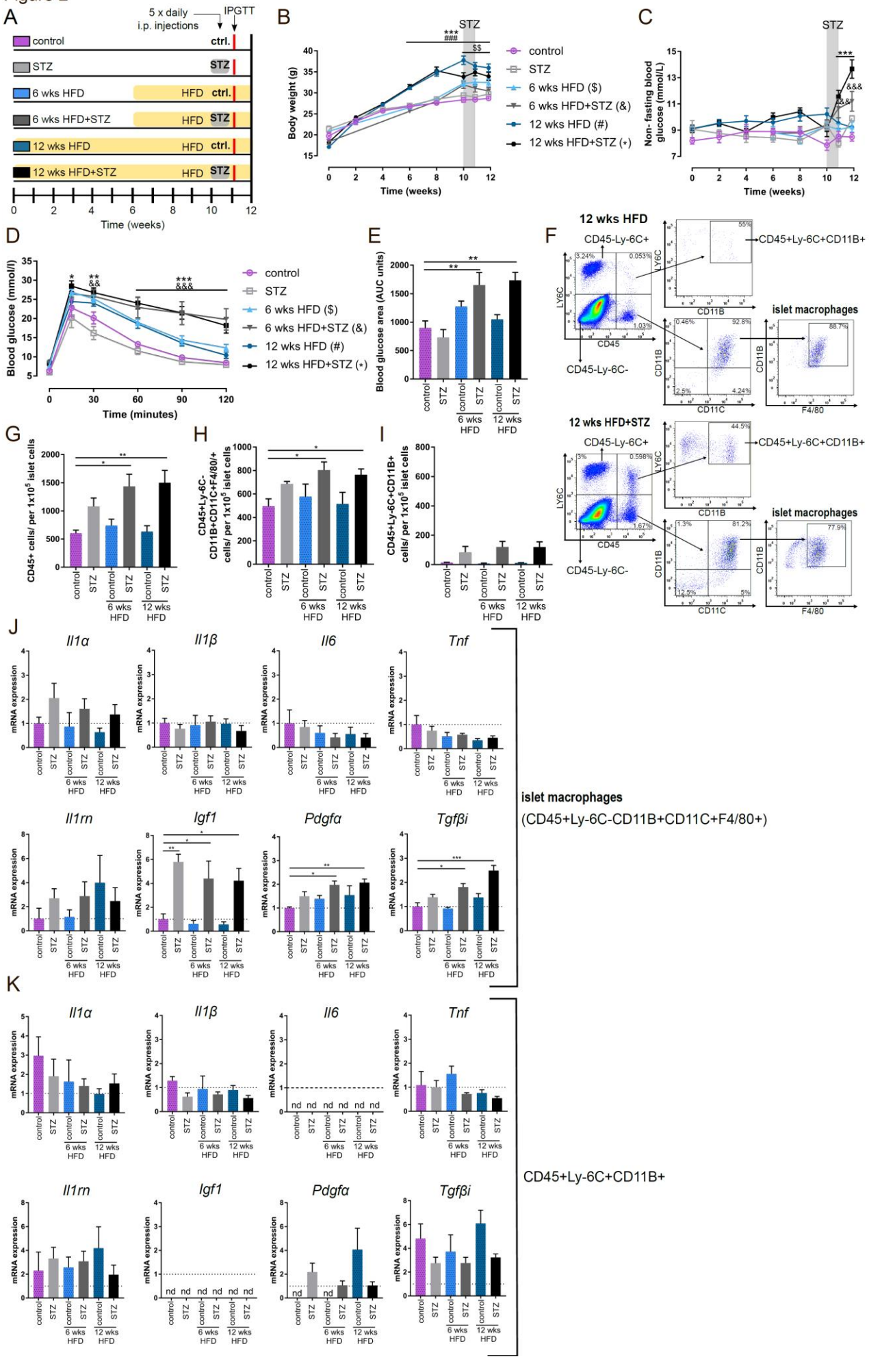

Figure 2

Islet macrophages in mice challenged with multiple low-dose STZ and high fat diet express increased *Igf1, Pdgfa, and Tgfbi*.

(A) Experimental design. C57BL/6J male mice were fed regular chow or HFD for 6 or 12 weeks. Multiple low doses of STZ (30 mg/kg, 5 x daily i.p. injections) or control buffer (acetate buffer, 5 x daily i.p. injections) were administered two weeks before sacrifice.

(B) Body weights; n=12-22 mice/group, $^{\&\&}p < 0.01$, $^{\#\#\#/}***p < 0.001$ versus control, two-way ANOVA with Dunnett's multiple comparisons test.

(C) Non-fasting blood glucose measurements; n=12-22 mice/ group, $^{\&\&}p < 0.01$, $^{\&\&\&/}***p < 0.001$ versus control, two-way ANOVA with Dunnett's multiple comparisons test.

(D) Glucose tolerance test (IPGTT, 1.5 g/kg) one week after administration of the first dose of STZ or vehicle control; n=7-9 mice/ group, $*p < 0.05$, $^{\&\&/}**p < 0.01$, $^{\&\&\&/}***p < 0.001$ versus control, two-way ANOVA with Dunnett's multiple comparisons test.

(E) Incremental area under the curve (AUC) for mice in (D); $**p < 0.01$ versus control, one-way ANOVA with Dunnett's multiple comparisons test.

(F) Representative flow cytometry plots and gating strategy for cell sorting of dispersed islets from mice that received HFD for 12 weeks with acetate buffer injections (top panel) or with multiple low-dose STZ injections (lower panel).

Fractions of (G) CD45+ cells, (H) CD45+Ly-6C-CD11B+CD11C+F4/80+ cells, (I) CD45+Ly-6C+CD11B+ cells from mice described in (A); n=5 for control, STZ groups; n=4 for 6 weeks HFD, 6 weeks HFD+STZ groups; n=5-6 for 12 weeks HFD, 12 weeks HFD+STZ groups.

(J-K) qPCR of islet macrophages (H) and CD45+Ly-6c+CD11B+ cells (I). Relative mRNA expression levels of *Il1α*, *Il1β*, *Tnf*, *Il6*, *Il1rn*, *Igf1*, *Pdgfα*, and *Tgfβi* expressed as fold over islet

macrophage control; n=4-6. For each sorting sample (n) islets from 3 mice were pooled together (average of 828 +/- 164 islets).

(G-K) *p < 0.05, **p < 0.01, ***p < 0.001 versus control, one-way ANOVA with Dunnett's multiple comparisons test.

Bar graphs or data points represent mean ± SEM.

See also Figure S2.

Figure 3

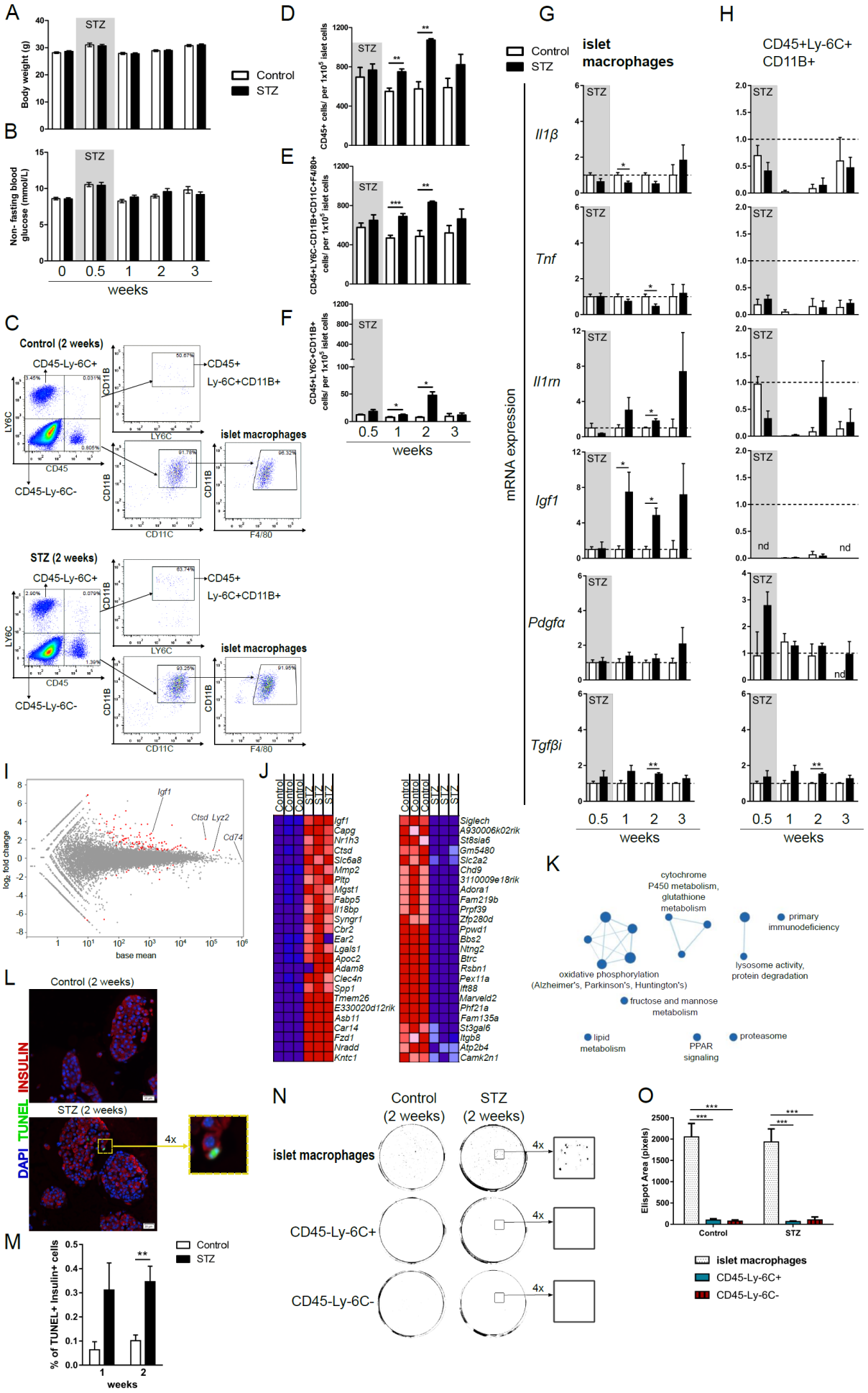

Figure 3

Islet macrophages in mice challenged with multiple low-dose STZ exhibit a gene shift towards enhanced metabolism and secrete IGF-1.

C57BL/6J male mice were given multiple low-dose STZ (30 mg/kg, 5 x daily i.p. injections) or control treatments (acetate buffer, i.p. injections) at 16-20 weeks of age.

(A) Body weights; n=9-11 mice/group.

(B) Non-fasting blood glucose levels; n=9-11 mice/group.

(C) Representative flow cytometry plots and gating strategy for cell sorting of dispersed islets from mice treated with multiple low-dose STZ (lower panel) or control treatments (top panel). Islets shown here were harvested two weeks after the first i.p. injection.

Fractions of (D) CD45+ cells, (E) CD45+Ly-6C-CD11B+CD11C+F4/80+ cells, (F) CD45+Ly-6C+CD11B+ cells.

(G-H) qPCR of islet macrophages (E) and CD45+Ly-6c+CD11B+ cells (F). Relative mRNA expression levels of *Il1β*, *Tnf*, *Il1rn*, *Igf1*, *Pdgfα*, and *Tgfβi* expressed as fold over islet macrophage control; n=3 for 0.5, 2, and 3-week treatments, and n= 5 for 1-week treatment. (D-H) For each sorting sample (n), islets were pooled from 2-4 mice (average of 911 +/- 198 islets).

(A-H) *p < 0.05, **p < 0.01, ***p < 0.001 versus corresponding control, Student's t test.

(I-K) Transcriptome analysis of islet macrophages from mice treated with multiple low-dose STZ or control. Islets from 10 mice were pooled to create each sorting sample (n); n= 3, average of 2314 +/- 200 islets.

(I) MA plot of genes (red points) shown to be differentially expressed between STZ and control.

(J) Heat map of RNA-seq results showing top 25 enriched genes in STZ (left panel) and top 25 enriched genes in control (right panel) islet macrophages following multiple low-dose STZ treatments (prepared with GSEA; red, pink, light blue, dark blue corresponds to the range of expression values- high, moderate, low, lowest).

(K) Network analysis of genes enriched in islet macrophages from STZ treated mice. Enrichment map of the top-ranking clusters of genes altered in STZ group with FDR $q < 0.05$ prepared with Cytoscape.

(L) Representative sections of TUNEL+, insulin+ cells harvested from control or multiple low dose STZ treated mice after 2 weeks from the start of treatment. Quantification is presented in (Figure 3L). DAPI stain is shown in blue, insulin is red and TUNEL is visualized as a green color; scale bar=20μm. On the right, outlined region is enlarged 4 times.

(M) Quantification of TUNEL+, insulin+ cells harvested from control or multiple low-dose STZ treated mice after 1 and 2 weeks from the start of treatment. Between 567-9870 nuclei per section were counted; n=3-5, $^{**}p < 0.01$ versus corresponding control, Student's t test.

(N) Representative IGF-1 ELISPOT images from cells sorted from dispersed islets. Two weeks after the first injection of buffer or multiple low-dose STZ, 2500 cells per group were sorted and analyzed by IGF-1 ELISPOT assay. On the right, outlined regions are enlarged 4 times.

(O) Quantification of (M) IGF-1 ELISPOT area in pixels; n= 6, $^{***}p < 0.001$ versus control, one-way ANOVA with Dunnett's multiple comparisons test.

Bar graphs or data points represent mean ± SEM.

Figure 4

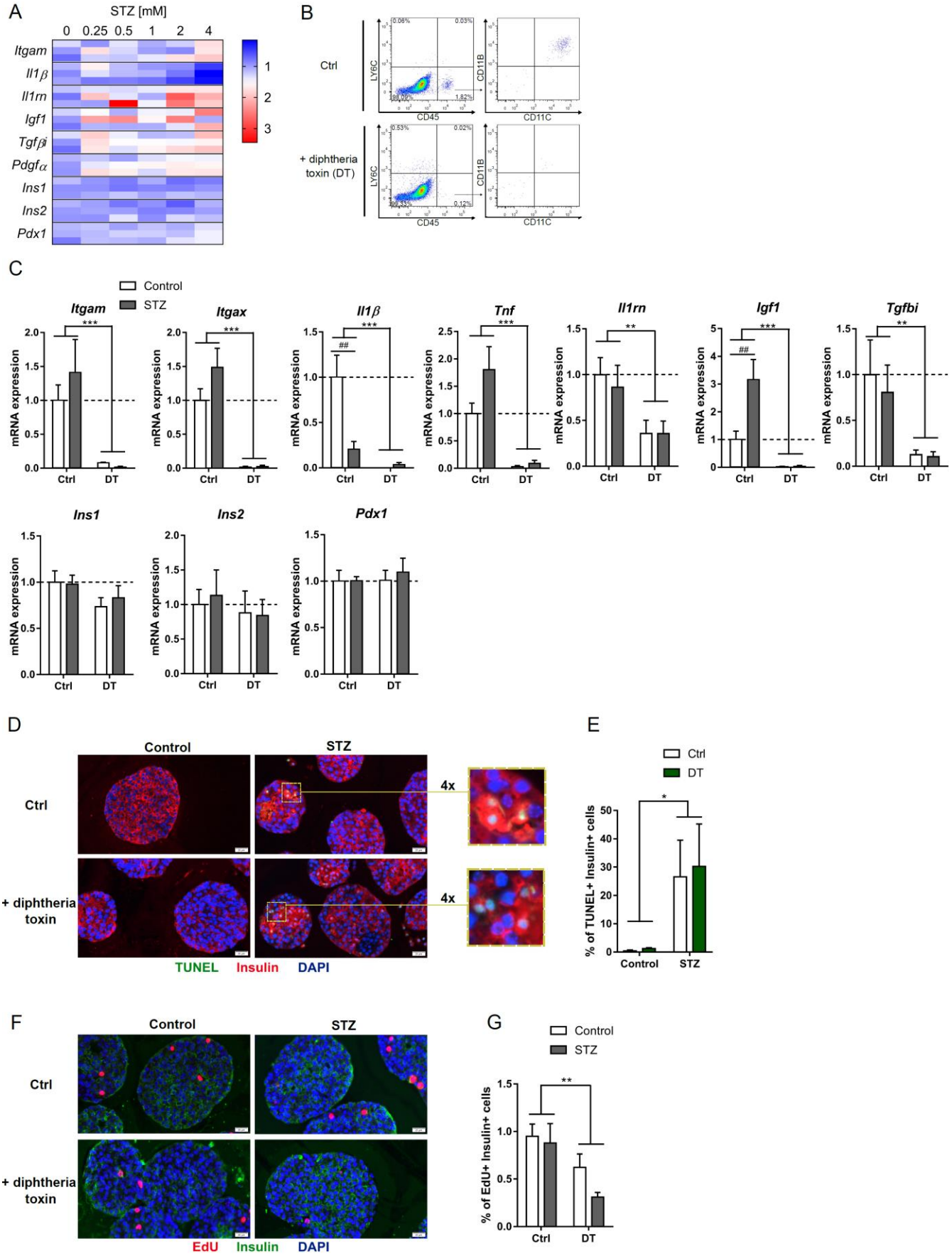

Figure 4

Islet macrophage depletion decreases Igf1 expression and beta-cell proliferation following STZ-induced beta-cell death *ex vivo*.

(A) qPCR of islets from male C57Bl/6 mice incubated *in vitro* with increasing doses of STZ for 40 min followed by 48 h recovery in islet media; n= 3, *p < 0.05 for Itgam (4 mM STZ), Pdgfa (2 and 4 mM STZ), Pdx1 (4 mM STZ), **p < 0.01 for Il1b (4mM STZ), Tgfbi (0.25 and 4 mM STZ) versus 0 mM STZ, one-way ANOVA with Dunnett's multiple comparisons test.

(B) Representative flow cytometry plots of dispersed islets from male CD11c-DTR mice depleted or not of islet macrophages.

(C) qPCR of islets from male CD11c-DTR mice depleted (DT) or not (Ctrl) of islet macrophages followed by treatment with 4 mM STZ (STZ, dark grey) or acetate buffer control (Control, white); n= 4-5, **p < 0.01, ***p < 0.001 versus Ctrl, $^{\#\#}$p < 0.01 versus Control, two-way ANOVA with Bonferroni's multiple comparisons test.

(D) Representative sections of TUNEL+ CD11c-DTR islets depleted (+ diphtheria toxin) or not (Ctrl) of islet macrophages followed by treatment with 4 mM STZ or acetate buffer control. Color scheme: DAPI- blue, insulin- red, TUNEL- green; scale bar=20µm.

(E) Quantification of (D). Between 544-4232 nuclei per section were counted. At least two sections from each sample (n) were counted; n=4, *p < 0.05 versus control, two-way ANOVA with Bonferroni's multiple comparisons test.

(F) Representative sections of EdU-treated CD11c-DTR islets depleted (+ diphtheria toxin) or not (Ctrl) of islet macrophages followed by treatment with 4 mM STZ or acetate buffer control. Color scheme: DAPI- blue, insulin- green, EdU- red; scale bar=20µm.

(G) Quantification of (F). Between 1412-3959 nuclei per section were counted. At least two sections from each sample (n) were quantified; n=3-5, **p < 0.01 versus Ctrl, two-way ANOVA with Bonferroni's multiple comparisons test.

Figure 5

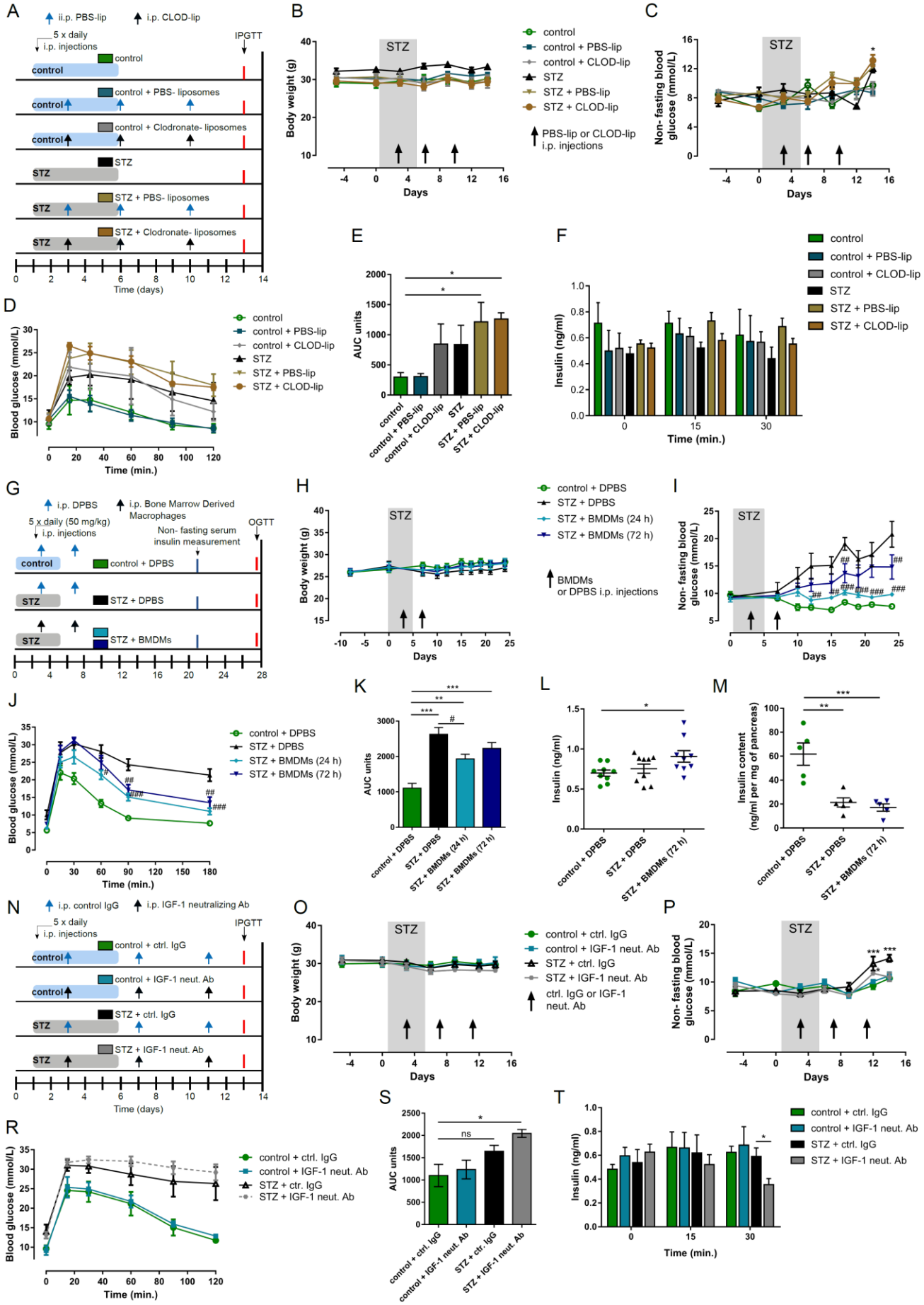

Figure 5

Macrophages and IGF-1 positively regulate glucose homeostasis in mice following multiple low-dose STZ.

(A) Experimental design of macrophage depletion study displayed in (B-F). Multiple low-dose STZ (30 mg/kg, 5 x daily i.p. injections) or control (acetate buffer, 5 x daily i.p. injections) treatments were administered to C57BL/6J males two weeks before sacrifice. 200 µl of Clodronate-loaded liposomes (Clod-lip) or PBS-loaded liposomes (PBS-lip) were injected i.p. on day 3, 6, and 10 from the first dose of STZ/buffer.

(B) Body weights; n=5 mice/control, control + PBS-lip, STZ + PBS-lip, STZ + CLOD-lip groups; n=4 mice/ STZ group, and n=3 mice/control + CLOD-lip group.

(C) Non-fasting blood glucose measurements; n=5 mice/control, control + PBS-lip, STZ + PBS-lip, STZ + CLOD-lip groups; n= 4 mice/STZ group, and n=3 mice/control + CLOD-lip group, **$p < 0.01$ for control versus STZ + CLOD-lip, two-way ANOVA with Dunnett's multiple comparisons test.

(D) Intraperitoneal glucose tolerance test (IPGTT, 1 g glucose/kg body weight) 13 days following the first dose of STZ/acetate buffer; n=5 mice/ control, control + PBS-lip, STZ + PBS-lip, STZ + CLOD-lip groups; n=4 mice/ STZ group, and n=3 mice/control + CLOD-lip group.

(E) Incremental area under the curve (AUC) for mice in (D); n=5 mice/control, control + PBS-lip, STZ + PBS-lip, STZ + CLOD-lip groups; n= 4 mice/STZ group, and n=3 mice/control + CLOD-lip group, *$p < 0.05$ versus control, one-way ANOVA with Dunnett's multiple comparisons test.

(F) Serum insulin levels. Blood was collected at time 0, 15, and 30 min during IPGTT shown in (D); n=5 mice/control, control + PBS-lip, STZ + PBS-lip, STZ + CLOD-lip groups; n= 4 mice/STZ group, and n=3 mice/control + CLOD-lip group.

(G) Design of experiments (H-M) involving adoptive transfer of bone-marrow derived macrophages (BMDMs). Multiple low-dose STZ (50 mg/kg, 5 x daily i.p. injections) or control (acetate buffer, 5 x daily i.p. injections) treatments were administered to C57BL/6J males four weeks before sacrifice. BMDMs that were starved of L929-conditioned medium for either 24 h or 72 h were injected i.p. on day 3 and 7 from the first dose of STZ/buffer.

(H) Body weights; n= 5-6 mice/group.

(I) Non-fasting blood glucose measurements; n= 5-6 mice/ group, $^{\#\#}p < 0.01$, $^{\#\#\#}p < 0.001$ versus STZ + DPBS, two-way ANOVA with Bonferroni's multiple comparisons test.

(J) Oral glucose tolerance test (OGTT, 2 g glucose/kg body weight) 25-26 days following administration of the first dose of STZ or acetate buffer; n= 5-6 mice, $^{\#}p < 0.05$, $^{\#\#}p < 0.01$, $^{\#\#\#}p < 0.001$ versus STZ + DPBS, two-way ANOVA with Bonferroni's multiple comparisons test.

(K) Incremental area under the curve (AUC) for mice in (P), n=5-6 mice/group, $^{**}p < 0.01$, $^{***}p < 0.001$ versus control + DPBS, $^{\#}p < 0.05$ versus STZ + DPBS, One-way ANOVA with Bonferroni's multiple comparisons test.

(L) Non-fasting serum insulin levels on day 21 following first dose of STZ/acetate buffer; n= 9, $^{*}p < 0.05$ versus control + DPBS, one-way ANOVA with Dunnett's multiple comparisons test.

(M) Pancreatic insulin content on day 27 following first dose of STZ/buffer; n= 5, $^{**}p < 0.01$, $^{***}p < 0.001$ versus control + DPBS, one-way ANOVA with Dunnett's multiple comparisons test).

See also Figure S4.

(N) Design of IGF-1 neutralization experiments (O-T). Multiple low-dose STZ (30 mg/kg, 5 x daily i.p. injections) or control (acetate buffer, 5 x daily i.p. injections) treatments were administered to C57BL/6J males two weeks before sacrifice. IGF-1 neutralizing antibody (0.1

µg/g body weight) or control IgG was injected i.p. on day 3, 7, and 11 following the first dose of STZ/buffer.

(O) Body weights; n= 5 mice/group.

(P) Non-fasting blood glucose measurements; n= 5 mice/group, *p < 0.05, **p < 0.01 versus control + ctrl. IgG, two-way ANOVA with Dunnett's multiple comparisons test.

(R) Intraperitoneal glucose tolerance test (IPGTT, 1.5 g glucose/kg body weight) 13 days following the first dose of STZ or acetate buffer; n=5 mice, most of the blood glucose readings in STZ + IGF-1 neut. Ab group were above the range of the glucose meter and were recorded as 33.3 mmol/L- the highest reading within the range of the glucose meter.

(S) Incremental area under the curve (AUC) for mice in (D); n=5, *p < 0.05 versus control + ctrl. IgG, Kruskal-Wallis test with Dunn's multiple comparisons test.

(T) Serum insulin levels. Blood was collected at time 0, 15, and 30 min during IPGTT showed in (D); n=5, *p < 0.05 versus STZ+ ctrl. IgG at 30 min, Student's t test.

Bar graphs or data points represent mean ± SEM.

STAR Methods

Experimental Model and Subject Details

Mice

BKS.Cg-Dock7m +/+ Leprdb/J (*db/db*), C57BLKS/J (BKS), B6.FVB-1700016L21Rik$^{Tg(Itgax-DTR/EGFP)57Lan}$/J (CD11c- DTR) and C57BL/6J mice were purchased from Jackson Laboratory (Bar Harbor, ME). Mice were housed and bred (C57BL/6J and Cd11c-DTR) in the BC Children's Hospital Research Institute Animal Care Facility in compliance with Canadian Council on Animal

Care guidelines with a 12h light/12h dark cycle and fed *ad libitum* chow diet or where indicated high fat diet (58 kcal% fat w/sucrose Surwit Diet). BKS and *db/db* males were 6-11 weeks old at the time of sacrifice. Islets from approximately 20-week-old CD11c-DTR males were used in experiments. 16-21-week-old C57BL/6J males were used in all studies using 30 mg/kg of streptozotocin (STZ), and 10-12-week-old C57BL/6J males were used in experiments using 50 mg/kg of STZ. Mice were given either 30 mg/kg STZ or acetate buffer (control) i.p. for 5 consecutive days, or for 2 consecutive days if sacrificed on day 3. Following the first STZ or buffer injection mice were sacrificed as indicated in figures on day 3, 7 or 14 and islets were isolated by collagenase digestion. *In vivo* IGF-1 neutralization was achieved by injecting IGF-1 neutralizing antibody at 0.1 µg/g body weight i.p.. Macrophages were depleted *in vivo* using clodronate loaded liposomes (or PBS loaded liposomes as controls) from Dr. Nico van Rooijen. Liposomes were allowed to reach room temperature, loaded into syringes, and the syringes inverted at least 10 times prior to injecting 200 µl of the solution i.p. per mouse. To adoptively transfer bone-marrow derived macrophages (BMDMs), mice were treated with either 50 mg/kg STZ or acetate buffer (control) i.p. for 5 consecutive days and ~0.5 x 10^6 BMDMs were injected i.p. on day 3 followed by injection of ~1 x 10^6 BMDMs i.p. on day 7 from the start of STZ/ buffer treatment. Mice were sacrificed on day 28 post STZ/buffer treatment. The numbers of animals studied are specified in each experiment. The University of British Columbia Animal Care Committee approved all animal studies.

Mouse Islet Culture

After isolation, mouse islets were cultured in islet medium (RPMI 1640 medium (11.1 mM glucose, 2 mM L-Glutamine, Phenol Red) containing 10% FBS, 2 mM L-alanyl-L-glutamine dipeptide (GlutaMAX), 1% penicillin/streptomycin, 10 µg/ml of gentamicin) at 37°C in 5% CO_2 and allowed to recover overnight prior to any *in vitro* experiments. For all *in vitro* experiments, 120-140 healthy-looking islets (round shape, absence of necrotic core, uniform brownish color)

from multiple age matched males were pooled together for each n. To determine the optimal dose of STZ *in vitro*, islets were subjected to increasing concentrations of STZ in Krebs Ringer Bicarbonate Buffer (KRB) for 40 min and returned to mouse islet media for 48 h. Corresponding concentrations of acetate buffer were used as controls. To deplete CD11c cells from Cd11c-DTR islets, 10 ng/ml of diphtheria toxin was added to cultured islets for 24 h. Thereafter, islets were treated with 4 mM of STZ or acetate buffer in KRB for 40 min and returned to mouse islet media with 10 ng/ml of diphtheria toxin or vehicle (0.9% NaCl) for 48 h.

Bone-Marrow Derived Macrophages (BMDMs)

Bone marrow was spun down out of mouse femurs and tibias and BMDMs prepared as previously reported (Nackiewicz et al 2014). Red Blood Cell Lysis solution (0.155 M NH_4Cl, 10 mM $KHCO_3$, 0.127 mM EDTA) was used to deplete erythrocytes and the remaining cells were passed through 40 µm pore size strainers. Around 6 x 10^6 cells were plated in 12 ml of DMEM supplemented with 1% penicillin/streptomycin, 10 mM HEPES, 10% FBS, and 15% L929-conditioned media in each 100 mm non-tissue culture treated dish and maintained at 37°C in 5% CO_2. Fresh medium was added on days 3 and 5. On day 7, vigorous pipetting with Cell Dissociation Buffer was used to detach adherent BMDMs. Cells were plated in DMEM supplemented with 1% penicillin/streptomycin, 10% FBS at a density described in figures. After 24 h, BMDMs were used in experiments. BMDMs that were starved of L929 conditioned medium for either 24 h or 72 h were used in adoptive transfer experiments.

Method Details

Islet Isolation

Mice anesthetized with isoflurane were sacrificed by cervical dislocation and islets isolated as previously reported (Nackiewicz et al 2014). After clamping the common bile duct, the pancreas was injected intraductally with approximately 2 mL of collagenase XI (1000 U/ml) in Hanks balanced salt-solution (HBSS) and placed in 50 mL tubes with an additional 3 mL of collagenase solution. The tube was incubated at 37°C for 14 minutes followed by gentle shaking to obtain a homogenously dispersed pancreas. Digestion was stopped with cold HBSS supplemented with 1 mM calcium chloride ($CaCl_2$). Islets were washed two times in cold HBSS with $CaCl_2$ and filtered through a 70 µM prewetted cell strainer. After flushing with 20 mL of HBSS with $CaCl_2$, the strainer was turned upside-down over a Petri dish and rinsed with 10 mL of islet media to wash the islets into the dish. Islets were handpicked under the Nikon SMZ800 microscope into a fresh Petri dish with islet media.

Physiological Measurements

Non-fasting blood glucose levels were measured from tail bleeds at room temperature using a hand-held blood glucose meter and test strips (OneTouch® UltraMini®, OneTouch® Ultra®2, OneTouch® Ultra® Blue Test Strips, LifeScan Canada). Body weights were recorded at the same time. Mice were fasted 5 hours and injected intraperitoneally (i.p) with 1.5 g glucose/kg of body weight or 1 g glucose/kg of body weight for i.p. glucose tolerance tests (IPGTT), or mice were given 2 g of glucose/kg of body weight for oral glucose tolerance tests (OGTT). Area under the curve (AUC) was calculated from baseline (time 0 min) for each animal and then used to determine the mean. Blood glucose levels during GTTs were measured from saphenous bleeds just before glucose injection and after 15, 30, 60 and 120 mins. Blood for serum insulin measurement was collected during 0, 15, and 30 min and measured using ELISA (Alpco). For plasma glucagon levels, aprotinin (250 kallikrein inhibitor units/mL plasma; Sigma-Aldrich) and dipeptidyl peptidase-4 inhibitor (50 µmol/L; Millipore) were added to the collection tubes and measured by ELISA (Mercodia).

Immunocytochemistry

Isolated islets were fixed with 4% paraformaldehyde for 15 minutes at room temperature, washed with DPBS, set in agarose, embedded in paraffin and sectioned. Apoptosis was assessed by TUNEL staining with the In Situ Cell Death Detection Kit (Roche) according to the manufacturer's directions. Proliferation was determined by EdU incorporation (islets were incubated with 10 µM EdU in islet media for 48 h or 72 h prior the fixation) and using the Click-iT™ EdU Alexa Fluor™ 594 Imaging Kit (Invitrogen) following the manufacturer's directions. Islet sections were blocked for 30 minutes at room temperature in 2% normal goat serum, incubated overnight at 4 °C with polyclonal guinea pig anti-insulin antibody (1:100 in 1% BSA in DPBS, DAKO) followed by 1 h room temperature incubation either with Alexa Fluor® 488 AffiniPure donkey anti-guinea pig or with DyLight™ 594 AffiniPure donkey anti-guinea pig secondary antibody (1:100 in 1% BSA in DPBS, Jackson ImmunoResearch Laboratories) and mounted using Vectashield with DAPI (Vector Laboratories). Imaging was acquired with a BX61 microscope and quantified using virtual slide microscope OlyVIA, ImageJ software and Image-Pro Analyzer.

Pancreatic insulin content

Mice were sacrificed, and the pancreas was isolated. A small piece from the pancreatic tail was excised, weighed, homogenized in acid ethanol, and extracted overnight at 4˚C. Samples were spun to remove debris. Supernatants were diluted, and insulin content measured by Insulin ELISA (Alpco).

Flow Cytometry and Cell Sorting

Islet macrophages were sorted as previously published (Nackiewicz et al 2014) with additional antibodies used to differentiate recruited monocytes. Freshly isolated islets were dispersed in

0.02% Trypsin-EDTA for 3 minutes followed by up to 1 minute of pipetting under a stereomicroscope to obtain a single cell solution. Islet media was added to stop the reaction. Dispersed islets were washed with FACS buffer (1% heat inactivated FBS, 1 mM EDTA, 11 mM glucose in PBS). Cells were kept on ice and pre-incubated with Fc Block (1:100) for 5 minutes, followed by 30 min incubation with CD45-eFluor 450 (1:250; clone 30-F11), Ly-6C-APC (1:1,200; clone HK1.4), CD11b-PE (1:1,200; clone M1/700, F4/80-FITC (1:150; clone BM8), CD11c-PECy7 (1:150; clone N418), and the viability dye 7AAD (1:2,000). Unstained, single stains, and fluorescence minus one controls were used for setting gates and compensation, and cells were gated on single, live cells. The detailed gating strategy is shown in figures. A BD LSR II was used for flow cytometry and a BD Aria IIu instrument (BD Biosciences) was used for cell sorting with the help of the BC Children's Hospital Research Institute FACS core facility.

ELISPOT

Islets from 2 C57BL/6J males aged 16-20 weeks were pooled to obtain enough macrophages for one sample (n). Mice were treated 14 days earlier with 5 daily i.p. injections of 30 mg/kg STZ or acetate buffer and cell sorting was performed as described above. 2500 cells from each group were sorted, plated for 40 h on a 96-well PVDF plate pre-coated with IGF-1 capture antibody (Peprotech Inc.) and maintained in islet media at 37°C in 5% CO_2. To detect secreted IGF-1, biotinylated anti-murine IGF-1 (Peprotech Inc.) and streptavidin-ALP were used according to the manufacturer's instructions. BMDMs served as a positive control. The plate was developed with BCIP/NBT substrate and read on an EliSpot reader AID Autoimmun Diagnostika GMBH (Germany). Spots were quantified with Image-Pro Analyzer. Pictures were converted to black and white and the number of pixels per well were measured. For visualization the black and white colors were inverted.

Real-Time PCR

Total RNA was isolated from whole islets and BMDMs using the NucleoSpin® RNA II kit (Macherey-Nagel), and from FACS-sorted cells using the RNeasy Micro Kit (Qiagen) following the manufacturer's instructions. RNA was quantified using a NanoDrop 2000c (Thermo Scientific). cDNA from whole islets and BMDMs was generated using Superscript II (Invitrogen). cDNA from FACS-sorted cells was prepared using Superscript III (Invitrogen). Quantitative PCR was performed using PrimeTime primers and probes (Integrated DNA Technologies) and TaqMan MasterMix (ThermoFisher/ Applied Biosystems) in the ViiA7 Real-Time PCR System (ThermoFisher/ Applied Biosystems). Differential gene expression was determined by the $2^{-\Delta\Delta Ct}$ method with *Rplp0* used as a reference gene.

Bulk RNA-seq

Male C57BL/6J mice aged 16-20 weeks were given either 30 mg/kg STZ or acetate buffer i.p. for 5 consecutive days. On day 14 following the first STZ/buffer injection mice were sacrificed and islets isolated. Islets from 10 mice were pooled per sample (n). Islets were hand-picked under the microscope, dispersed, and FACS-sorted as described above. Viable, single CD45+Ly6c-Cd11b+Cd11c+F4/80+ cells were sorted using a BD FACS Aria IIu directly into lysis buffer, and the RNeasy Plus Micro Kit from Qiagen was used to isolate total RNA. Total RNA quality control quantification was performed using an Agilent 2100 Bioanalyzer. All RNA samples had an RNA integrity number (RIN) ≥9.1. The NeoPrep Library Prep System (TruSeq Stranded mRNA Kit) from Ilumina was used for library preparation followed by sequencing using standard Illumina methods and Ilumina NextSeq500. RNA-Seq Alignment (BaseSpace Workflow) 1.0.0, TopHat (Aligner) 2.1.0, were used to map raw reads to the reference genome of Mus musculus (UCSC mm10). Cufflinks 2.2.1, BLAST 2.2.26+, DEseq2 (Love et al., 2014), VisR (Younesy et al., 2015), gene set enrichment analysis (GSEA 3.0, the pathway gene sets: gseaftp.broadinstitute.org://pub/gsea/gene_sets_final/c2.cp.v6.2.symbols.gmt, Subramanian et al., 2005, Mootha et al., 2003,) were used to analyze the transcriptome. Cytoscape v3.7.0 with

the enrichment map plugin was used to generate a gene set enrichment map based on GSEA analysis. A node cut-off Q-value of 0.05 and an edge cut-off of 0.5 were used.

Quantification and Statistical Analysis

Statistical Analysis

Data are reported as mean ± SEM. Statistical analysis with normality tests were performed, and graphs were created with GraphPad Prism version 7.00. Two-tailed Student's t test was used when comparing two means. One-way ANOVA or Kruskal-Wallis test with Dunn's multiple comparisons test was applied when comparing more than two groups, and two-way ANOVA was used when comparing two independent variables in at least two groups. To compare every mean with a control, mean Dunnett's post-test was employed. Bonferroni's post-hoc test was used to compare a set of means. Differences were considered significant at $p<0.05$. The n value and details on statistical analyses of each experiment are indicated in the figure legends.

Data and Software Availability

Data Resources

RNA-seq data have been deposited in the ArrayExpress database at EMBL-EBI (www.ebi.ac.uk/arrayexpress) under accession number E-MTAB-7234.

KEY RESOURCES TABLE

REAGENT or RESOURCE	SOURCE	IDENTIFIER
Antibodies		
CD45 Monoclonal Antibody (30-F11), eFluor 450	ThermoFisher/ eBioscience	48-0451-82, RRID: AB_1518806
Ly-6C Monoclonal Antibody (HK1.4), APC	ThermoFisher/ eBioscience	17-5932-82, RRID: AB_1724153
CD11b Monoclonal Antibody (M1/70), PE	ThermoFisher/ eBioscience	12-0112-82, RRID: AB_2734869
CD11c Monoclonal Antibody (N418), PE-Cyanine7	ThermoFisher/ eBioscience	25-0114-82, RRID: AB_469590
F4/80 Monoclonal Antibody (BM8), FITC	ThermoFisher/ eBioscience	11-4801-82, RRID: AB_2637191
CD16/CD32 Monoclonal Antibody (93) Fc Block	ThermoFisher/ eBioscience	14-0161-85, RRID: AB_467134
Polyclonal Guinea Pig Anti-Insulin	Dako	A0564, RRID: AB_10013624
Alexa Fluor® 488 AffiniPure Donkey Anti-Guinea Pig IgG (H+L)	Jackson ImmunoResearch Laboratories Inc.	706-545-148, RRID: AB_2340472
DyLight™ 594 AffiniPure F(ab')$_2$ Fragment Donkey Anti-Guinea Pig IgG (H+L)	Jackson ImmunoResearch Laboratories Inc.	706-516-148, RRID: AB_2340471
Goat Anti-Mouse IGF-1 Antigen Affinity-purified Polyclonal Antibody (for neutralization)	R&D Systems	AF791, RRID: AB_2248752
Normal Goat IgG Control	R&D Systems	AB-108-C, RRID: AB_354267
Anti-Murine IGF-1	Peprotech Inc.	500-P157G
Biotinylated Anti-Murine IGF-1	Peprotech Inc.	500-P157GBt, RRID: AB_2737301
Bacterial and Virus Strains		
None		
Biological Samples		
None		
Chemicals, Peptides, and Recombinant Proteins		
7-AAD (7-Aminoactinomycin D)	ThermoFisher/ Invitrogen	A1310
HBSS (10X), no calcium, no magnesium, no phenol red	ThermoFisher/ Gibco	14185052
Collagenase from Clostridium histolyticum, Type XI, 2-5 FALGPA units/mg solid, ≥800 CDU/mg solid	Sigma- Aldrich/ Millipore Sigma	C7657
RPMI 1640 Medium	ThermoFisher/ Gibco	11875119
DMEM Medium	ThermoFisher/ Gibco	11995065

DPBS, no calcium, no magnesium	ThermoFisher/ Gibco	14190144
Gentamicin (10 mg/mL)	ThermoFisher/ Gibco	15710064
GlutaMAX™ Supplement	ThermoFisher/ Gibco	35050061
Penicillin-Streptomycin (10,000 U/mL)	ThermoFisher/ Gibco	15140122
Fetal Bovine Serum, qualified, heat inactivated, Canada origin	ThermoFisher/ Gibco	12484028
Cell Dissociation Buffer, enzyme-free, Hanks' Balanced Salt Solution	ThermoFisher/ Gibco	13150016
Trypsin-EDTA (0.25%), phenol red	ThermoFisher/ Gibco	25200056
Recombinant Murine IGF-1	Peprotech Inc.	250-19
RNaseOUT™ Recombinant Ribonuclease Inhibitor	ThermoFisher/ Invitrogen	10777019
Streptozocin, ≥75% α-anomer basis, ≥98% (HPLC), powder	Sigma- Aldrich/ Millipore Sigma	S0130
Diphtheria Toxin, Unnicked, *Corynebacterium diphtheriae*	EMD Millipore/ Calbiochem	322326
UltraPure™ DNase/RNase-Free Distilled Water	ThermoFisher/ Invitrogen	10977-015
Agarose	Fisher Scientific	BP160-500
VECTASHIELD Antifade Mounting Medium with DAPI	Vector Laboratories	H-1200
Critical Commercial Assays		
RNeasy Micro Kit	QIAGEN	74004
RNeasy Plus Micro Kit	QIAGEN	74034
NucleoSpin® RNA II	Macherey-Nagel	740955.250
rDNase Set	Macherey-Nagel	740963
SuperScript™ II Reverse Transcriptase	ThermoFisher/ Invitrogen	18064-014
SuperScript™ III Reverse Transcriptase	ThermoFisher/ Invitrogen	18080-044
TaqMan™ Universal Master Mix II, no UNG	ThermoFisher/ Applied Biosystems	4440040
TaqMan™ Fast Advanced Master Mix	ThermoFisher/ Applied Biosystems	4444557
Murine IGF-1 Standard ABTS ELISA Development Kit	Peprotech Inc	900-K170
Mouse Ultrasensitive Insulin ELISA	Alpco	80-INSMSU-E01
STELLUX Rodent Insulin ELISA	Alpco	80-INSMR-CH01
Click-iT™ EdU Alexa Fluor™ 594 Imaging Kit	ThermoFisher/ Invitrogen	C10339
In Situ Cell Death Detection Kit, Fluorescein	Sigma- Aldrich/ Millipore Sigma/ Roche	11684795910

Mercodia Glucagon ELISA	Mercodia	10-1281-01
Deposited Data		
RNAseq	This paper	EMBL-EBI E-MTAB-7234
Experimental Models: Cell Lines		
None		
Experimental Models: Organisms/Strains		
Mouse: C57BLKS/J	The Jackson Laboratory	JAX stock #000662
Mouse: BKS.Cg-Dock7^{m} +/+ Lepr^{db}/J	The Jackson Laboratory	JAX stock #000642
Mouse: B6.FVB-1700016L21Rik$^{Tg(Itgax-DTR/EGFP)57Lan}$/J	The Jackson Laboratory	JAX stock #004509
Mouse: C57BL/6J	The Jackson Laboratory	JAX stock #000664
Oligonucleotides		
50 nm Random Hexamer, sequence: NNNNNN	IDT	rmrndm
dNTP Set (100 mM)	ThermoFisher/ Invitrogen	10297-018
Rplp0 Probe: 5'-/56-FAM/TGTCTTCCC/ZEN/TGGGCATCACGTC/3IABkFQ/-3' Primer 1: 5'-TGACATCGTCTTTAAACCCCG-3' Primer 2: 5'-TGTCTGCTCCCACAATGAAG-3'	IDT	N/A
Il1α Probe: 5'-/56-FAM/TCCAACCCA/ZEN/GATCAGCACCTTACAC/3IABkFQ/-3' Primer 1: 5'-TGCAGTCCATAACCCATGATC-3' Primer 2: 5'-ACAAACTTCTGCCTGACGAG-3'	IDT	N/A
Il1β Probe: 5'-/56-FAM/AGAGCATCC/ZEN/AGCTTCAAATCTCGCA/3IABkFQ/-3' Primer 1: 5'-ACGGACCCCAAAAGATGAAG-3' Primer 2: 5'-TTCTCCACAGCCACAATGAG-3'	IDT	N/A
Il1rn Probe: 5'-/56-FAM/TCATAGTGT/ZEN/GTTCTTGGGCATCCACG/3IABkFQ/-3' Primer 1: 5'-TCATTGCTGGGTACTTACAAGG-3' Primer 2: 5'-ATCTCCAGACTTGGCACAAG-3'	IDT	N/A

Tnf Probe: 5'-/56-FAM/ATCTGAGTG/ZEN/TGAGGGTCTGGGC/3IABkFQ/-3' Primer 1: 5'-CTTCTGTCTACTGAACTTCGGG-3' Primer 2: 5'-CAGGCTTGTCACTCGAATTTTG-3'	IDT	N/A
Il6 Probe: 5'-/56-FAM/CCTACCCCA/ZEN/ATTTCCAATGCTCTCCT/3IABkFQ/-3' Primer 1: 5'-CAAAGCCAGAGTCCTTCAGAG-3' Primer 2: 5'-GTCCTTAGCCACTCCTTCTG-3'	IDT	N/A
Igf1 Probe: 5'-/56-FAM/AGAAGTCCC/ZEN/CGTCCCTATCGACA/3IABkFQ/-3' Primer 1: 5'-GAGACTGGAGATGTACTGTGC-3' Primer 2: 5'-CTCCTTTGCAGCTTCGTTTTC-3'	IDT	N/A
Tgfβi Probe: 5'-/56-FAM/TGTGCGACT/ZEN/TGCCCCTGTCTATC/3IABkFQ/-3' Primer 1: 5'-AACCGACCACAAGAACGAG-3' Primer 2: 5'-GCTTCATCCTCTCCAGTAACC-3'	IDT	N/A
Pdgfα Probe: 5'-/56-FAM/CGCAGGAAG/ZEN/AGAAGTATTGAGGAAGCC/3IABkFQ/-3' Primer 1: 5'-TTAACCATGTGCCCGAGAAG-3' Primer 2: 5'-ATCAGGAAGTTGGCCGATG-3'	IDT	N/A
Itgam Probe: 5'-/56-FAM/CCACACTCT/ZEN/GTCCAAAGCCTTTTGC/3IABkFQ/-3' Primer 1: 5'-CATCCCATGACCTTCCAAGAG-3' Primer 2: 5'-GTGCTGTAGTCACACTGGTAG-3'	IDT	N/A
Itgax Probe: 5'-/56-FAM/ACACAGGCC/ZEN/GGGAGAAGCAA/3IABkFQ/-3' Primer 1: 5'-TTCAAGGAGACAAAGACCCG-3' Primer 2: 5'-AGAGAAAAGTTGAGGCGAAGAG-3'	IDT	N/A
Pdx1 Probe: 5'-/56-FAM/ACAAGAGGA/ZEN/CCCGTACTGCCTACA/3IABkFQ/-3' Primer 1: 5'-CCCTTTCCCGTGGATGAAATC-3' Primer 2: 5'-GAATTCCTTCTCCAGCTCCAG-3'	IDT	N/A

Ins1 Probe: 5'-/56-FAM/TGTTGGTGC/ZEN/ACTTCCTACCCCTG/3IABkFQ/ -3' Primer 1: 5'-ATCAGAGACCATCAGCAAGC-3' Primer 2: 5'-GTTTGACAAAAGCCTGGGTG-3'	IDT	N/A
Ins2 Probe: 5'-/56-FAM/CCTCCACCC/ZEN/AGCTCCAGTTGT/3IABkFQ/-3' Primer 1: 5'-GGCTTCTTCTACACACCCATG-3' Primer 2: 5'-TGATCTACAATGCCACGCTTC-3'	IDT	N/A
Recombinant DNA		
None		
Software and Algorithms		
FlowJo 7.6	https://www.flowjo.com/solutions/flowjo	RRID: SCR_008520
BD FACSDiva 6	http://www.bdbiosciences.com	
OlyVIA 2.8	https://www.olympus-lifescience.com/	RRID:SCR_016167
GraphPad Prism 7	http://www.graphpad.com/	RRID:SCR_002798
Image-Pro Analyzer 6.2	http://www.mediacy.com/	
ImageJ software	https://imagej.nih.gov/ij/	RRID: SCR_003070
Gene Set Enrichment Analysis (GSEA) 3.0	https://www.broadinstitute.org/gsea	RRID:SCR_003199
DESeq2	https://bioconductor.org/packages/release/bioc/html/DESeq2.html	RRID:SCR_015687
VisR 0.9.37	https://visrsoftware.github.io/	RRID:SCR_016658
Cytoscape v3.7.0	https://cytoscape.org/	RRID:SCR_003032
Other		
PBS Liposomes and Clodronate Liposomes	www.ClodronateLiposomes.com	N/A
58 kcal% fat w/sucrose Surwit Diet	Research Diets	D12331
OneTouch Ultra® test strips	LifeScan	Blue, code 25
OneTouch Ultra® UltraMini®, OneTouch® Ultra2® blood glucose meters	LifeScan	N/A
Fisherbrand™ Microhematocrit Capillary Tubes, Heparinized	Fisher Scientific	22-362566
Fisherbrand™ Microhematocrit Capillary Tubes, Not Heparinized	Fisher Scientific	22-362574

Falcon™ Cell Strainer, 40 µm	Fisher Scientific/ Corning Life Sciences	08-771-1
Falcon™ Cell Strainer, 70 µm	Fisher Scientific/ Corning Life Sciences	08-771-2
L929 conditioned media	AbLab, Biomedical Research Centre, Core Media Facility-Vancouver, UBC	N/A

Contact for Reagent and Resource Sharing

Further information and requests for reagents may be directed to and will be fulfilled by the corresponding author, Dr. C. Bruce Verchere (bverchere@bcchr.ca).

Supplemental Figures

Figure S1

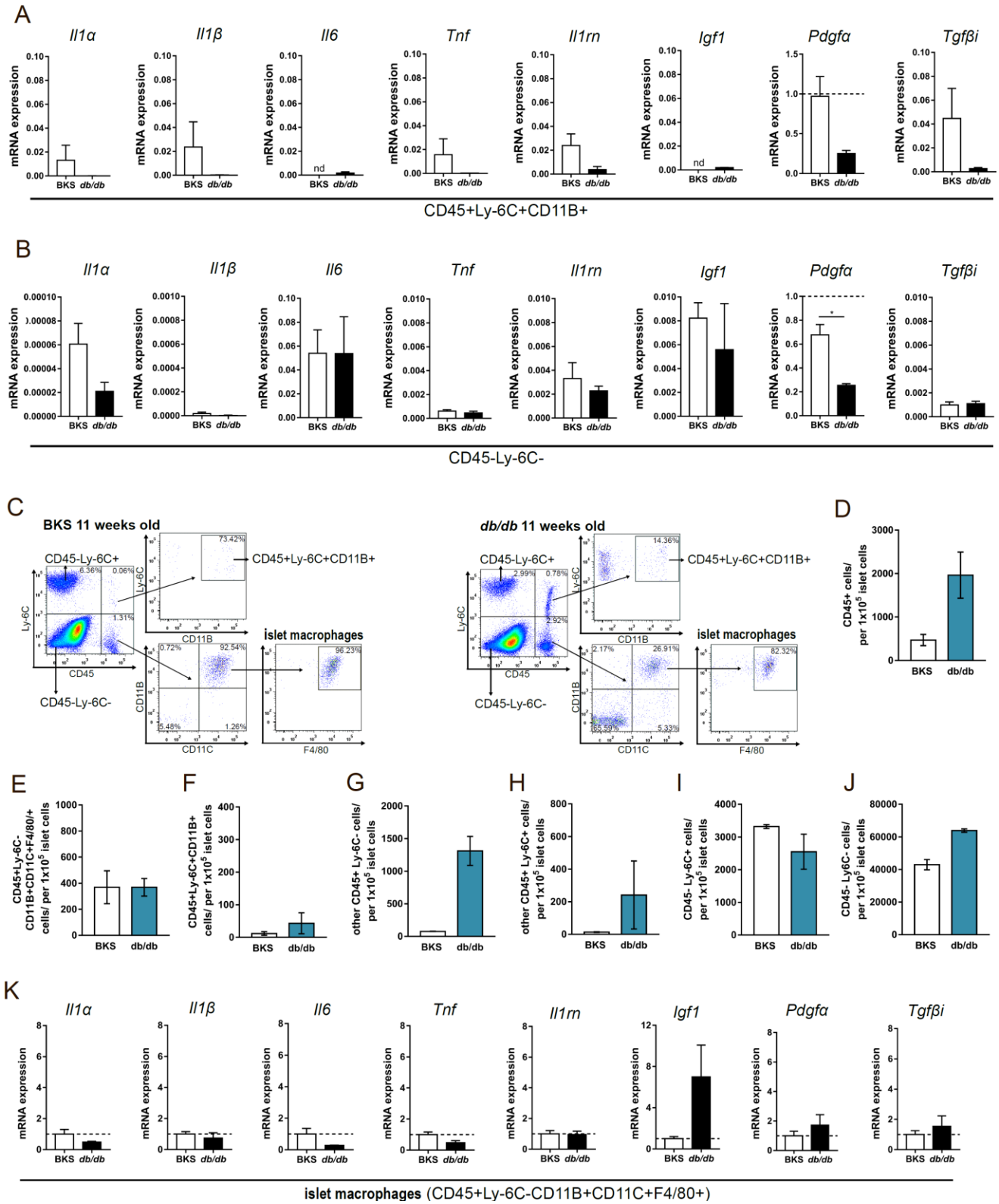

Figure S1

Islet immune cell populations and mRNA expression in 8- and 11-week old diabetic *db/db* mice.

(A) qPCR of CD45+Ly-6C+CD11B+ cells (Figure 1H), and (B) qPCR of CD45-Ly-6C- cells (Figure 1L) from 8-week-old BKS and db/db mice. Relative expression levels of *Il1α*, *Il1β*, *Tnf*, *Il6*, *Il1rn*, *Igf1*, *Pdgfα*, and *Tgfβi* presented as fold control BKS islet macrophages (CD45+Ly-6C-CD11B+CD11C+F4/80+); n=4, 2-4 mice pooled per sample (n); *p < 0.05, Student's t test.

(C) Representative flow cytometry profiles and gating strategy for cell sorting of dispersed islets from 11-week-old BKS and db/db mice.

Fractions of (D) CD45+ cells, (E) CD45+Ly-6C-CD11B+ CD11C+F4/80+ cells, (F) CD45+Ly-6C+CD11B+ cells, (G) other CD45+Ly-6C- cells, (H) other CD45+Ly-6C+ cells, (I) CD45-Ly-6C+ cells, (J) and CD45-Ly-6C- cells in 11-week-old BKS and db/db mice.

(K) qPCR of islet macrophages (E). Relative expression levels of *Il1α*, *Il1β*, *Tnf*, *Il6*, *Il1rn*, *Igf1*, *Pdgfα*, and *Tgfβi* shown as fold control (BKS).

(D-K) For BKS mice, 2 mice per sample were pooled to obtain 520 +/- 26 islets and 4 sorting samples in total, n=4; for *db/db* mice, 4-5 mice were pooled to obtain 464 +/- 127 islets and 2 sorting samples in total, n=2.

Figure S2

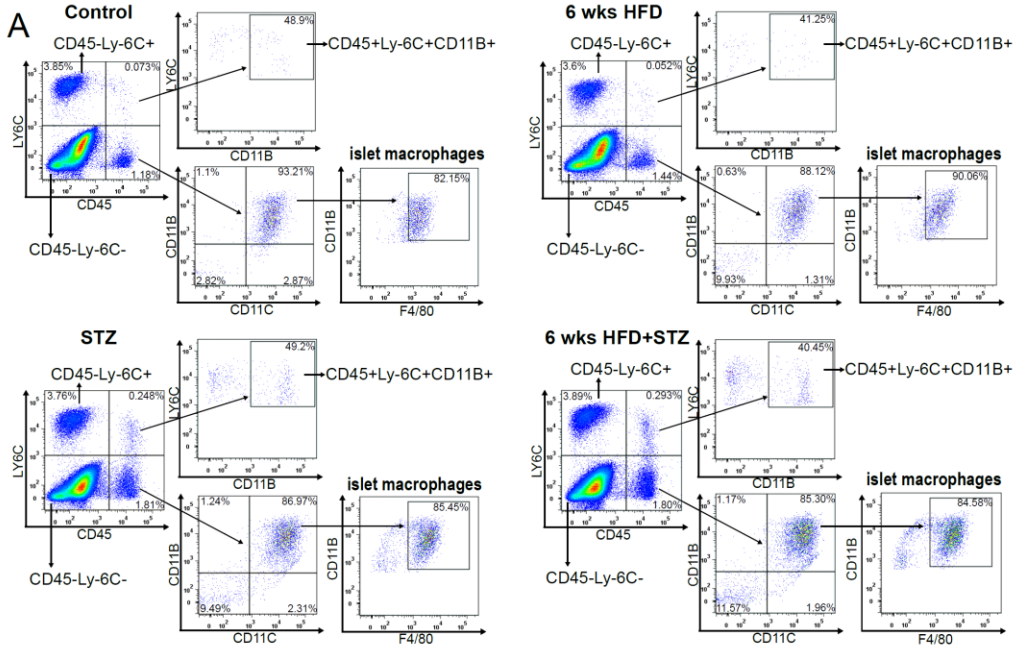

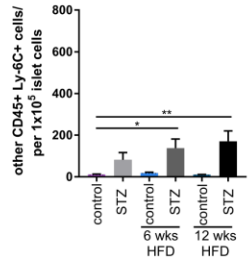

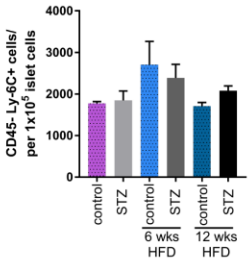

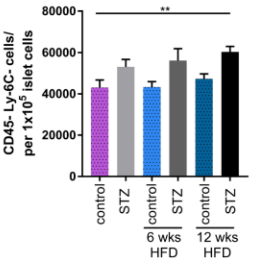

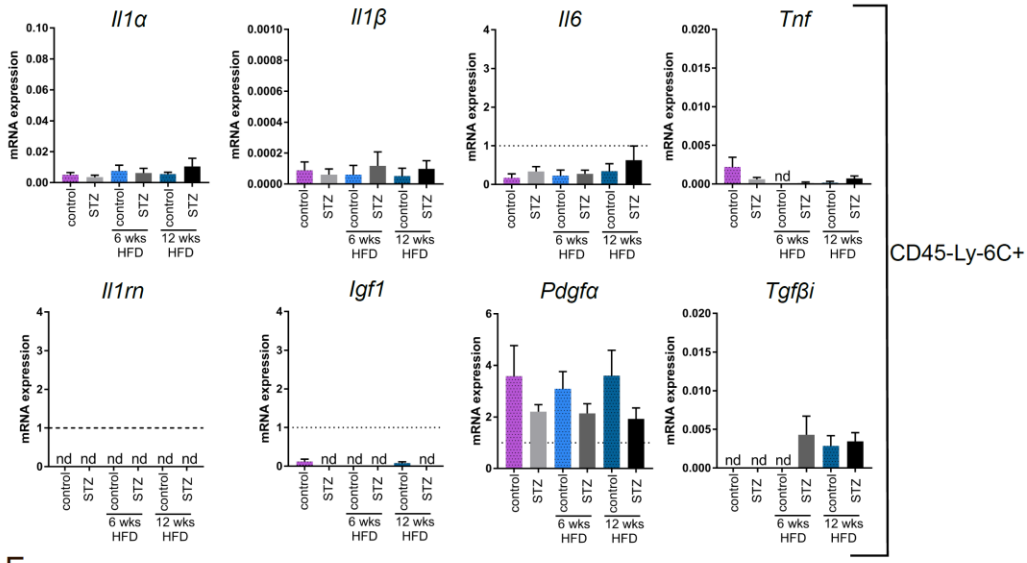

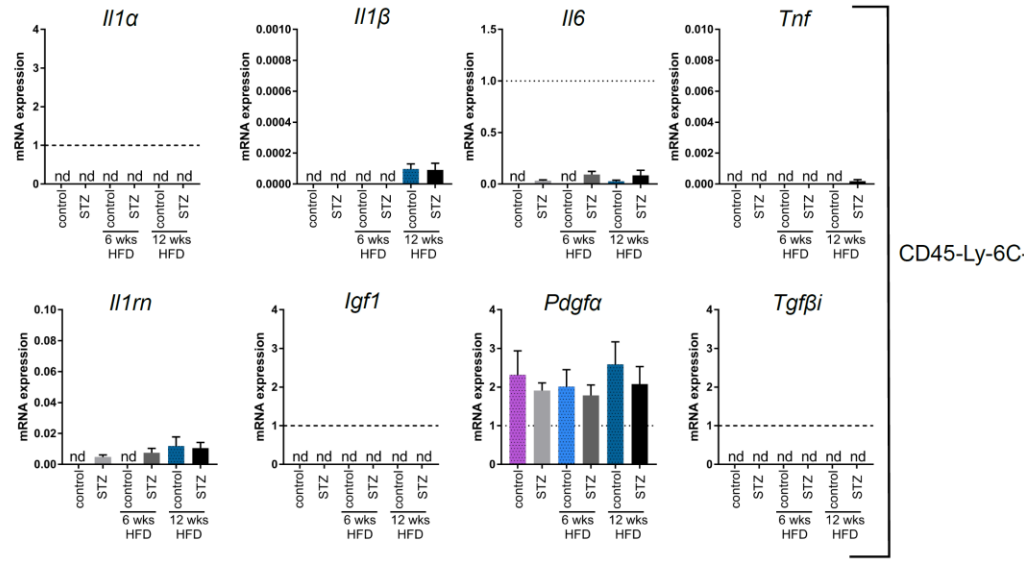

Figure S2

Islet immune cell populations and mRNA expression in mice challenged with multiple low-dose STZ and HFD.

(A) Representative flow cytometry plots of dispersed islets from mice in control (upper left panel), STZ (lower left panel), 6 wks HFD (upper right panel), and 6 wks HFD+STZ (lower right panel) groups.

Fractions of (B) other CD45+Ly-6C+ cells, (C) CD45-Ly-6C+ cells, (D) CD45-Ly-6C- cells; n= 5 for control, STZ groups; n=4 for 6 weeks HFD, 6 weeks HFD+ STZ groups; n= 5-6 for 12 weeks HFD, 12 weeks HFD+ STZ groups, *$p < 0.05$, **$p < 0.01$ versus control, one-way ANOVA with Dunnett's multiple comparisons test.

qPCR of (E) CD45-Ly-6C+ cells (C) and (F) CD45-Ly-6C- cells (D). Relative mRNA expression levels of *Il1α*, *Il1β*, *Tnf*, *Il6*, *Il1rn*, *Igf1*, *Pdgfα*, and *Tgfβi* illustrated as fold over control islet macrophages; n=4-6, 3 mice pooled per sample. No statistical significance was reached in (E) or (F).

Bar graphs or data points represent mean ± SEM.

nd- not detectable

Figure S3

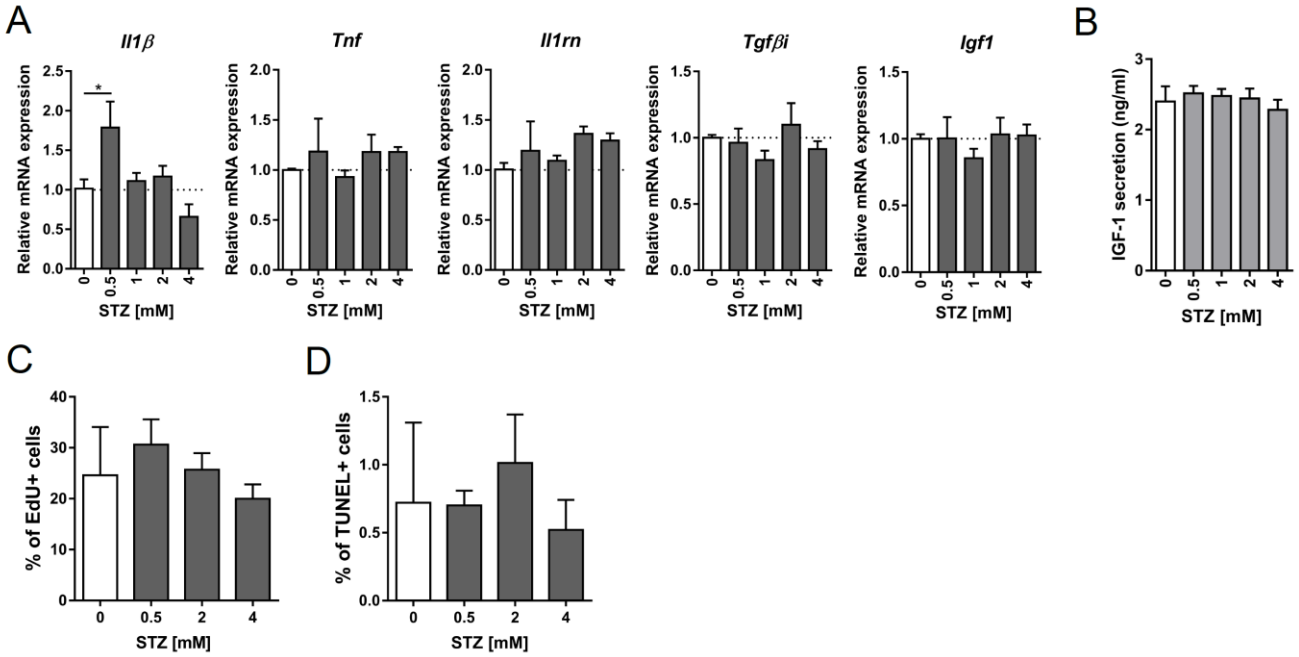

Figure S3

Bone marrow derived macrophages do not secrete IGF-1 following STZ treatment.

(A) qPCR of BMDMs incubated *in vitro* with increasing doses of STZ for 40 min followed by 48 h recovery in islet media. Relative mRNA expression levels of *Il1β*, *Tnf*, *Il1rn*, *Igf1*, and *Tgfβi* shown as fold over control; n= 3, *p < 0.05 versus 0 mM STZ, one-way ANOVA with Dunnett's multiple comparisons test.

(B) IGF-1 ELISA of BMDMs incubated *in vitro* with increasing doses of STZ for 40 min followed by 48 h recovery in islet media; n= 3.

(C) Quantification of TUNEL+ and (D) EdU+ BMDMs incubated *in vitro* with increasing doses of STZ for 40 min followed by 48 h recovery in islet media; n= 2.

Figure S4

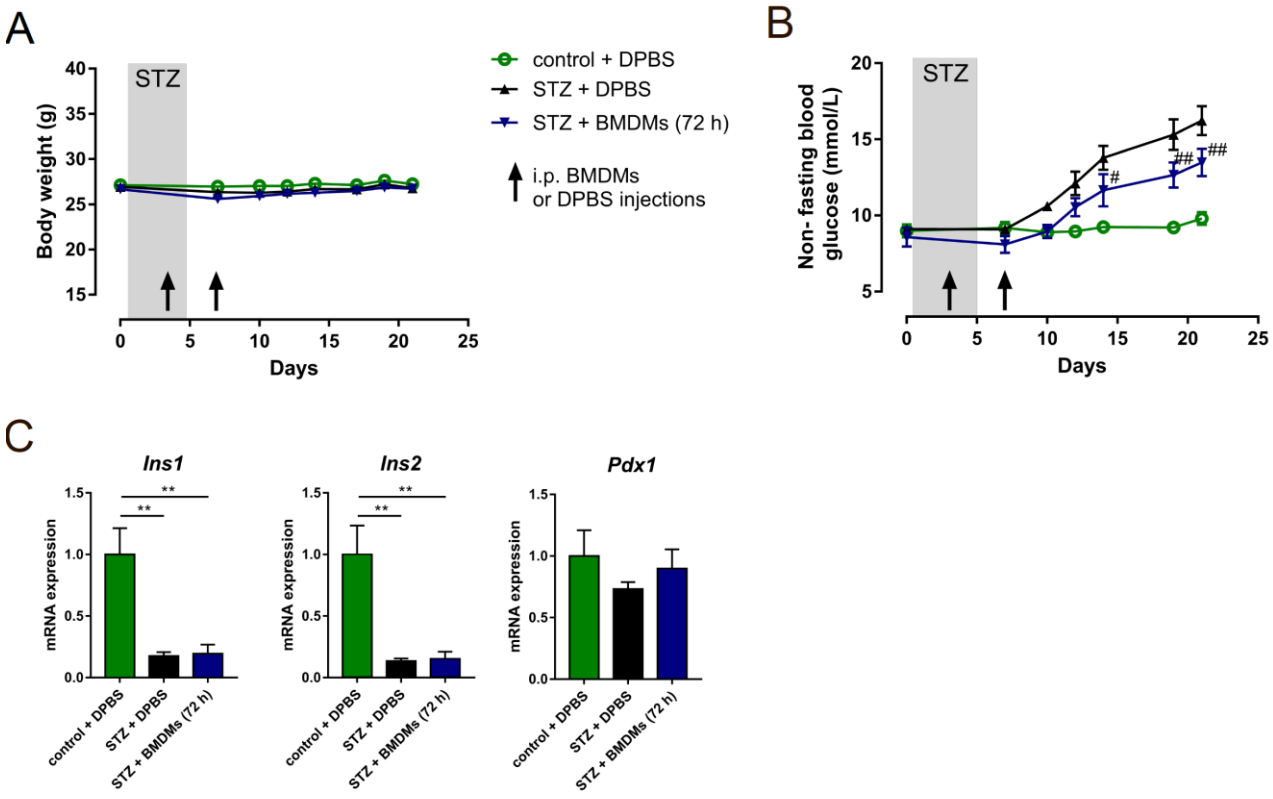

Figure S4

Adoptive transfer of BMDMs into STZ-treated mice lowers non-fasting blood glucose levels.

(A) Body weights of experimental mice described in Figures 5L-M; n= 9 mice/group.

(B) Non-fasting blood glucose levels of cohort described in (A); n= 9 mice/ group, $^{\#}p < 0.05$, $^{\#\#}p < 0.01$ versus STZ + DPBS, two-way ANOVA with Bonferroni's multiple comparisons test.

(C) qPCR of whole pancreatic mRNA on day 27 following first dose of STZ/ buffer. Relative mRNA expression levels of *Ins1, Ins2,* and *Pdx1* illustrated as fold over control; n= 5, **p < 0.01, versus control + DPBS, One-way ANOVA with Dunnett's multiple comparisons test.

Table S1

Gene sets enriched in STZ versus control treated islet macrophages with FDR q-value < 0.05.

NAME	SIZE	ES	NES	NOM p-val	FDR q-val	FWER p-val	RANK AT MAX	LEADING EDGE
KEGG_PPAR_SIGNALING_PATHWAY	37	0.605	2.203	0	0.040	0.000	355	tags=24%, list=3%, signal=25%
KEGG_ALZHEIMERS_DISEASE	130	0.628	2.194	0	0.040	0.040	1740	tags=54%, list=16%, signal=63%
KEGG_HUNTINGTONS_DISEASE	140	0.627	2.102	0	0.040	0.040	1740	tags=54%, list=16%, signal=64%
KEGG_LYSOSOME	108	0.574	2.043	0	0.040	0.040	1624	tags=40%, list=15%, signal=46%
KEGG_DRUG_METABOLISM_CYTOCHROME_P450	20	0.748	1.992	0	0.040	0.040	1189	tags=55%, list=11%, signal=61%
KEGG_GLYCOSAMINOGLYCAN_DEGRADATION	16	0.709	1.987	0	0.040	0.040	746	tags=44%, list=7%, signal=47%
REACTOME_GLUCONEOGENESIS	21	0.713	1.975	0	0.040	0.040	1658	tags=57%, list=15%, signal=67%
BIOCARTA_BAD_PATHWAY	22	0.569	1.952	0	0.040	0.040	438	tags=18%, list=4%, signal=19%
KEGG_PARKINSONS_DISEASE	97	0.707	1.932	0	0.045	0.091	1815	tags=69%, list=16%, signal=82%
REACTOME_REGULATION_OF_APOPTOSIS	54	0.635	1.930	0	0.045	0.091	2494	tags=63%, list=22%, signal=81%
KEGG_OXIDATIVE_PHOSPHORYLATION	100	0.744	1.923	0	0.044	0.091	1744	tags=72%, list=16%, signal=85%
KEGG_CARDIAC_MUSCLE_CONTRACTION	41	0.685	1.920	0	0.044	0.091	1876	tags=59%, list=17%, signal=70%
REACTOME_TCA_CYCLE_AND_RESPIRATORY_ELECTRON_TRANSPORT	107	0.713	1.908	0	0.044	0.091	1740	tags=68%, list=16%, signal=80%
REACTOME_CROSS_PRESENTATION_OF_SOLUBLE_EXOGENOUS_ANTIGENS_ENDOSOMES	44	0.665	1.897	0	0.043	0.091	2494	tags=70%, list=22%, signal=90%
KEGG_METABOLISM_OF_XENOBIOTICS_BY_CYTOCHROME_P450	18	0.794	1.893	0	0.043	0.091	1189	tags=67%, list=11%, signal=75%
REACTOME_ACTIVATION_OF_NF_KAPPAB_IN_B_CELLS	60	0.528	1.891	0	0.043	0.091	1917	tags=50%, list=17%, signal=60%
REACTOME_ANTIGEN_PRESENTATION_FOLDING_ASSEMBLY_AND_PEPTIDE_LOADING_OF_CLASS_I_MHC	15	0.565	1.890	0	0.043	0.091	2532	tags=53%, list=23%, signal=69%
REACTOME_ANTIGEN_PROCESSING_CROSS_PRESENTATION	64	0.641	1.876	0	0.043	0.091	2532	tags=64%, list=23%, signal=82%
REACTOME_DESTABILIZATION_OF_MRNA_BY_AUF1_HNRNP_D0	50	0.613	1.867	0	0.043	0.091	1917	tags=56%, list=17%, signal=67%
REACTOME_AUTODEGRADATION_OF_THE_E3_UBIQUITIN_LIGASE_COP1	46	0.679	1.867	0	0.042	0.091	2494	tags=72%, list=22%, signal=92%
REACTOME_P53_DEPENDENT_G1_DNA_DAMAGE_RESPONSE	51	0.656	1.852	0	0.045	0.091	2494	tags=69%, list=22%, signal=88%
REACTOME_CDK_MEDIATED_PHOSPHORYLATION_AND_REMOVAL_OF_CDC6	45	0.670	1.846	0	0.047	0.091	2494	tags=69%, list=22%, signal=88%
KEGG_ETHER_LIPID_METABOLISM	20	0.633	1.843	0	0.046	0.091	971	tags=25%, list=9%, signal=27%
REACTOME_LIPID_DIGESTION_MOBILIZATION_AND_TRANSPORT	25	0.575	1.842	0	0.046	0.091	1005	tags=28%, list=9%, signal=31%